Transforming NiCo2O4 nanorods into nanoparticles using citrus lemon juice enhancing electrochemical properties for asymmetric supercapacitor and water oxidation

Shusheel Kumar, Aneela Tahira, Adeel Liaquat Bhatti, Muhammad Ali Bhatti, Riaz Hussain Mari, Nek Muhammad Shaikh, Muhammad Yameen Solangi, Ayman Nafady, Mélanie Emo, Brigitte Vigolo, et al.

Transforming $NiCo_2O_4$ nanorods into nanoparticles using citrus lemon juice enhancing electrochemical properties for asymmetric supercapacitor and water oxidation

Shusheel Kumar[a], Aneela Tahira[c], Adeel Liaquat Bhatti[a], Muhammad Ali Bhatti[d], Riaz Hussain Mari[a], Nek Muhammad Shaikh[a], Muhammad Yameen Solangi[e], Ayman Nafady[j], Mélanie Emo[f], Brigitte Vigolo[f], Antonia Infantes-Molina[g], Alberto Vomiero[*h,i], Zafar Hussain Ibupoto[*b]

[a]Institute of Physics, University of Sindh Jamshoro, 76080, Sindh Pakistan

[b]Institute of Chemistry, University of Sindh Jamshoro, 76080, Sindh Pakistan

[c]Institute of Chemistry, Shah Abdul Latif University Khairpur Mirs, Sindh, Pakistan

[d]Institute of Environmental Sciences, University of Sindh Jamshoro, 76080, Sindh Pakistan

[e]Mehran University of Engineering and Technology, 7680 Jamshoro, Sindh Pakistan

[f]Université de Lorraine, CNRS, IJL, F-54000 Nancy, France

[g]Department of Inorganic Chemistry, Crystallography and Mineralogy. (Unidad Asociada al ICP-CSIC), Faculty of Sciences, University of Malaga, Campus de Teatinos, 29071, Malaga, Spain

[h]Department of Engineering Sciences and Mathematics, Division of Material Science, Luleå University of Technology, Luleå, Sweden

[i]Department of Molecular Sciences and Nanosystems, Ca' Foscari University of Venice, Venezia Mestre, Italy

[j]Chemistry Department, College of Science, King Saud University, Riyadh, 11451, Saudi Arabia

***Corresponding authors**: Alberto Vomiero and Zafar Hussain Ibupoto

Email: alberto.vomiero@ltu.se , zaffar.ibhupoto@usindh.edu.pk

Abstract

Recently, the nanostructured nickel-cobalt bimetallic oxide ($NiCo_2O_4$) material with high electrochemical activity has received an intensive attention. Beside this, biomass assisted synthesis of $NiCo_2O_4$ is getting popularity due to advantageous features such as low cost, simple, minimum use of toxic chemicals, environment and ecofriendly The electrochemical activity of spinel $NiCo_2O_4$ is associated to mixed metal oxidation states. Therefore, large attention is paid on the crystal quality, morphology and tunable surface chemistry of $NiCo_2O_4$ nanostructures. In this study, we have used citrus lemon juice consisting variety of chemical compounds having properties of stabilizing agent, capping agent and chelating agent. Moreover, the presence of several acidic nature chemical compounds in citrus lemon juice have changed the pH of growth solution and consequently we observed the surface modified and structural changes which were found to be very effective for the development of energy conversion an energy storage systems. These naturally occurring compounds in citrus lemon juice have played a dynamic role in transforming the one dimensional (1D) nanorod morphology of $NiCo_2O_4$ to small and well packed zero dimensional (0D) nanoparticles. Hence, the prepared of $NiCo_2O_4$ nanostructures are exhibiting new surface-oriented nanoparticles, high defects on the surface (especially oxygen vacancies), sufficient ionic diffusion and reaction of electrolytic ions, enhanced electrical conductivity, and favorable reaction kinetics rate at the interface. The electrocatalytic properties of $NiCo_2O_4$ nanostructures were studied for the evaluation of oxygen evolution reaction (OER) at low overpotential of 250 mV for10 $mAcm^{-2}$, Tafel slope of 98 $mVdec^{-1}$, and durability of 40 h. Moreover, the asymmetric supercapacitor was investigated and obtained results indicated a high specific capacitance of (Cs) of 1519.19 Fg^{-1}, and energy density of 33.08 Wh kg^{-1} at 0.8 Ag^{-1}. The enhanced electrochemical performance could be attributed to the favorable structural changes, surface modification, and surface crystal facets exposure due to the use of citrus lemon juice. The proposed method of transformation of 1D nanorod to 0D nanoparticles could be used for the design of new generation of efficient electrocatalyst materials for energy storage and conversion uses.

Keywords: Citrus lemon juice, oxygenated groups, $NiCo_2O_4$ material, asymmetric supercapacitor, oxygen evolution reaction

1. Introduction

Currently, the supercapacitors are found highly effective electrochemical energy storage devices, hence significant advancement has been made in this field [1-3]. Supercapacitors have advantageous features including high energy density, long cycling durability, high power density and extended spectrum of operational temperature conditions in comparison to the conventional capacitors and regular electrochemical batteries [4-6]. Generally, there are two classes of supercapacitors described by charge-discharge behavior. First type is the electrochemical double layer capacitors (EDLCs), which stores charges on the basis of electrostatic approach on the active sites of electrode material on the basis of reversible adsorption of electrolytic ions. Second type is the pseudo-capacitors or redox supercapacitors, which stores the charges using fast and reversible redox processes [6]. For this reason, the preparation of unique architectures of nanostructured materials are highly desirable for the development of energy storage devices like supercapacitors (SCs). The use of spinel nickel-cobalt bimetallic oxide ($NiCo_2O_4$) can be seen as a strong candidate for oxygen evolution reaction (OER) and SCs due to its favorable variety of mixed oxidation states, fast charge transfer of electron and an excellent electrical conductivity [7-9]. It has been shown that the activity of $NiCo_2O_4$ material is highly depending on well oriented shape structures towards OER and SCs such as nanoparticles [10,11], microcuboids [12], hollow spheres [13], octahedrons [14], and nanocages [15]. The combustion of fossil fuels inherently produce large amount of greenhouse gases causing global warming effect ultimately polluted the environment [16, 17]. Hence, the handling of challenges of clean energy, and its storage are taken seriously by developing new functional materials. For the purpose of clean energy, various technologies are used such as hydropower, solar energy, airstream and biomass based fuel productions [18-20]. The water dissociation into hydrogen gas does not take place without the input of energy due to strong H-O chemical bonding, therefore theoretically a minimum voltage of 1.23 V is needed for the dissociation of water. Such a high energy is difficult to manage from the existing renewable energy sources or fossil fuels; therefore the synthesis of numerous electrocatalysts has been taken into consideration to lower the energy barrier for the water splitting [13-15]. Typically, the OER and HER reaction process take place at the anode and the cathode, respectively [21].

Among both reactions, OER is very challenging as it is accompanied by the transfer of four electrons and considered as bottleneck challenge for the exploitation of efficient hydrogen

production from water splitting [22-25, 26-27]. For this purpose, the most efficient electrocatalysts are noble metals, like Ru/Ir/Pt/Pd. However, their large scale utilization is limited due to high scarcity and cost [21]. To overcome this, low-cost and earth abundant electrocatalysts have been investigated belonging to transition metal-based materials [28-32]. The $NiCo_2O_4$ material nanostructures are widely used for OER owing to its high catalytic activity and electrical conductivity [33-35]. However, the performance of $NiCo_2O_4$ material is limited by the low density of catalytic sites and sluggish charge transfer rate at the interface of electrode and electrolyte. Furthermore, it has been shown that the electrochemical properties of $NiCo_2O_4$ are highly dependent on the shape, structure and desirable chemical composition [36, 37]. For this reason, an enhanced electrochemical activity of nanoplate like $NiCo_2O_4$ was observed [38]. Various factors effect on the morphological transformation of nanostructured material and electrochemical properties such as pH, temperature, surfactant, and synthetic routes have extensively studied [39]. Hence, it is a big challenge to prepare the different morphologies of $NiCo_2O_4$ for improved electrochemical performances.

The use of new synthetic methodologies demonstrated effective to increase the performance of $NiCo_2O_4$ nanostructures [40, 41]. The use of biomass for tuning the catalytic activity of $NiCo_2O_4$ nanostructured material is considered extensively these days, hence different biomasses have been used during the synthesis [40, 41]. Previous studies have used different biomasses consisting phytochemicals and they have modified the surface properties of $NiCo_2O_4$ nanostructures very effectively [40, 41]. Previously, the utilization of ascorbic acid and citric acid from citrus lemon juice has been carried out on the ZnO material and its phase transformation, morphology and optical properties [42]. The citrus lemon juice exhibits wide range of unique chemical compounds as could be seen from Supplementary Scheme 1 [43], and their molecular structure was drawn by king draw software. The scientific details of citrus lemons as tracheophyta (phylum), magnoliopsida (class), sapindales (order), rutaceae (family), and citrus limon/limonum (species). In this study, the use of citrus lemon was employed to alter the pH of growth solution in addition to provision of capping, reducing and stabilizing agents during the preparation of $NiCo_2O_4$ nanostructured material. Moreover, there is less attention paid about the citrus lemon juice to create surface oxygen vacancies, high Ni and Co oxidation states ratios, structural transformation, creating high surface active sites, high compatibility of $NiCo_2O_4$ nanostructured material with electrode, and these aspects of material design have not been

studied for the development of energy conversion and storage systems in the existing literature. Importantly, low cost, and simple method for the transformation of 1D nanorod to 0D nanoparticles bring an advancement in the field of nanoscience for the development of future generation of functional nanostructures for a wide range of applications. Therefore, keeping in view the natural product chemistry of citrus lemon juice, particularly citric acid, malic acid, and ascorbic acid, we have utilized them together for the first time to enhance the electrochemical performance of $NiCo_2O_4$ nanostructured material. Furthermore, the concept of terminal oxygenated groups through the use of variety of citrus lemon juice ingredients opens the new gateway for the synthesis of surface modified nanostructured materials with advanced functional properties. For this purpose, we have studied these types of aspects of citrus lemon juice on the $NiCo_2O_4$ nanostructured material towards efficient energy storage and OER applications for the first time.

In this research work, we have used a variety of oxygenated sites of various natural compounds of citrus lemon juice for the hydrothermal preparation of short range and well packed nanoparticles of $NiCo_2O_4$.

2. Experimental Section

2.1. Preparation of $NiCo_2O_4$ nanostructured material using citrus lemon juice

Nickel chloride hexahydrate, cobalt chloride hexahydrate, potassium hydroxide, ruthenium oxide (RuO_2), alumina paste of (0.3µM) and urea were of analytical grade and they were purchased from Sigma Aldrich Karachi, Sindh Pakistan. Fresh citrus lemon fruit was purchased from local market of Jamshoro, Sindh Pakistan. Prior to the synthesis of $NiCo_2O_4$ nanostructured material, the lemon juice was collected from the cleaned lemon fruit using Philips juicer machine. The preparation of $NiCo_2O_4$ nanostructured material was followed by two steps. First hydrothermal process was carried out to prepare bimetallic hydroxide phase, then thermal combustion was done in air to transform hydroxide phase into bimetallic oxide. A typical synthesis was initiated as follows: first, three beakers were taken and containing three main precursors concentrations of 0.015M nickel chloride hexahydrate, 0.1M cobalt chloride hexahydrate, and 0.1M urea were mixed in 100 mL of the deionized water. Two beakers were containing main precursors of nickel salt, cobalt salt and urea and successive addition of 0.5 mL, 1 mL and 2 mL of lemon juice was performed. They were labeled as sample 1, sample 2 and

sample 3 respectively. The fourth beaker was containing the growth precursors of nickel salt, cobalt salt and urea and it was labeled as pure sample of $NiCo_2O_4$ nanostructured material. The primary use of urea was to add certain value of hydroxyl ions in the growth solution to favor the formation of hydroxide phase of nickel-cobalt. Moreover, urea provides the hydroxyl ions through the release of ammonia which further reacts with the water and gives out hydroxyl ions for binding with metallic ions coming from their respective salt precursors. Whereas the use of citrus lemon was to change the pH of the growth solution in addition to supply capping, reducing and stabilizing agents during the preparation of $NiCo_2O_4$ nanostructured material. The relative acidic nature of several compounds like ascorbic acid, malic acid and citric acid existing in lemon juice can alter the pH of the solution. However, the relative amount of those acidic nature ingredients of lemon juice in the 1 mL and 2 mL samples could be very low but their presence in the growth solution has slightly changed the pH of growth solution. The pH of growth solution without the use of lemon was about 6.72 and the pH of the growth solution with the use of 0.5mL and 1mL of lemon juice was about 6.2 and 5.8 respectively. Whereas pH of growth solution with the use of 2 mL of lemon juice was found about 3.2. The significant variation in the pH of growth solutions with 0.5mL, 1mL and 2 mL of lemon juice could play a dynamic role to alter the structure and surface properties of the nanostructured material. Four beakers with growth solutions were sealed very tightly with aluminum foil and placed in electric oven for 5 hours at 95^oC. After the growth process, the hydroxide product of nickel-cobalt was collected onto filter paper and washed with the deionized water. Later, the product was dried and allowed for the thermal combustion treatment in air for 5 hours at 500^oC. At the end, we were successful to get a black product of $NiCo_2O_4$ nanostructured material including sample 1, sample 2, sample 3 and pure sample. The characterization of various $NiCo_2O_4$ nanostructured materials was done with respect to morphology, crystal arrays, chemical composition and surface defects using various analytical techniques. SEM was used to study morphology of $NiCo_2O_4$ nanostructures at applied voltage of 2 kV with a ZEISS Gemini SEM 500 equipped with a field emission gun. Powder X-ray diffraction was employed to identify the phase and purity of $NiCo_2O_4$ nanostructured material under the experimental conditions of X-rays with a wavelength of wavelength $\lambda_{K\alpha}$ = 1.5406 Å coming from Cu anode at applied potential of 45 kV and 45 mA current. Transmission and scanning transmission electron microscopy (TEM and STEM, respectively) observations were performed on a JEOL JEM - ARM 200F Cold FEG microscope

working at 200 kV and equipped with a probe corrector (Cs). Chemical analyses were done with energy dispersive X-ray spectroscopy (EDX) (SDD, Jeol DRY SD 30 GV). X-ray photoelectron spectroscopy (XPS) with X-ray source from Al K_α at 30 eV for the surface chemical composition analysis. The measured binding energies of as prepared $NiCo_2O_4$ nanostructured materials were fitted with the reference binding energy of C1s peak at 284.6 eV.

2.2. Electrochemical characterization of surface modified $NiCo_2O_4$ nanostructured material

We have tested different $NiCo_2O_4$ samples towards supercapacitor and OER half-cell water splitting applications in aqueous solution of KOH electrolyte. The supercapacitor investigations were performed with three electrode cell set up in 3.0M KOH. The reference electrode was based on calomel electrode (Hg/HgO), and graphite rod as counter electrode. The working electrode was glassy carbon electrode (GCE) with a diameter of 3.0 mm diameter and it was used for the deposition of $NiCo_2O_4$ nanostructured materials using drop casting approach. Before modification, the GCE was cleaned with the paste of 0.3µM alumina powder slurry and rubbed by silicon paper; consequently it was washed several times with the deionized water. The supercapacitor characterization was done with chronopotentiometry (CP) by measuring galvanostatic charge-discharge (GCD) curves at various current densities for the estimation of specific capacitance (C_s) F/g, cycling stability and energy density. The calculations of supercapacitor application are shown calculation (S1).

Furthermore, OER studies were performed on the different $NiCo_2O_4$ nanostructures in 1.M KOH. The catalyst ink of $NiCo_2O_4$ nanostructures was prepared by dispersing 5 mg of each sample in 4 mL of the deionized water and 100µL of 5% Nafion. The homogenous dispersion was obtained using sonication process for 10 min. Then, 5µL of each catalyst ink with approximately mass of (0.2mg) was deposited onto cleaned GCE using drop casting method and dried with the blow of air. The OER half-cell investigations were studied by different electrochemical modes like cyclic voltammetry (CV), linear sweep voltammetry (LSV), chronopotentiometry (CP) and electrochemical impedance spectroscopy (EIS). Prior to LSV measurement, three CV cycles were done at a scan rate of 10 mV/s for the measurement of stable LSV curves for OER process at a scan rate of 2 mV/s. The EIS measurement was used to measure the kinetics of charge transfer at the interface of modified electrode and electrolyte under the measurement conditions of sweeping frequency range from 100 kHz to 0.1 Hz using an amplitude of 5 mV and OER onset potential. The CV curves in the non-Faradic region at various scan rates were measured to

find the amount of active surface area using electrochemical active surface area (ECSA) calculations. The long-term durability was investigated by chronopotentiometry technique for the time period of 40 hours at a constant current density of 20 mA cm^{-1}. The measured potential against calomel reference electrodes was converted to reversible hydrogen electrode (RHE) by following the Nernst equation. The Tafel equation was used to find the Tafel slope values from the linear part of LSV curves for the illustration of reaction kinetics. All the energy storage and conversion measurements were carried out under standard conditions. The stepwise preparation methodology and electrochemical testing are shown in Scheme 1.

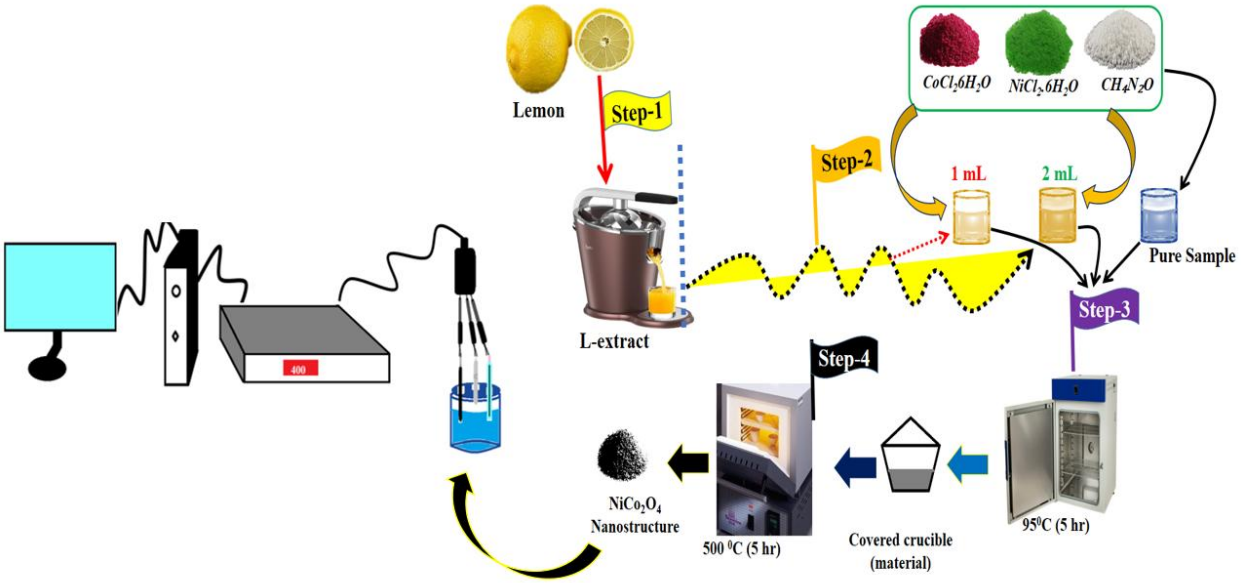

Scheme 1: Stepwise preparation of $NiCo_2O_4$ nanostructured material using lemon juice and their electrochemical testing set up

3. Results and discussion

3.1. Physical characterization of as prepared different $NiCo_2O_4$ nanostructures

Morphology and structure of the synthesized $NiCo_2O_4$ based nanocatalysts were studied by SEM and XRD, respectively (Figure 1). Figure 1a shows the typical shape orientation of pristine $NiCo_2O_4$ nanostructures prepared by hydrothermal process which is characterized by nanorod like morphology with a length of several microns and average diameter in the range of 300-500 nm. The morphology of nanorod is assembled by the nanoparticles with a dimension of below

100 nm as shown in Figure 1a, insert. Furthermore, the morphology of citrus lemon juice assisted $NiCo_2O_4$ nanostructures with volume of 1 mL (sample 2 Figure 1b) was found with different morphology from pure sample of $NiCo_2O_4$ nanostructured material. For both of them, 1D nanorod morphology was transformed into well packed small size 0D nanoparticles. The size of small size nanoparticles could be below 100 nm, which is a typical a nanostructured phase of as prepared $NiCo_2O_4$ nanostructures. The growth process in the presence of citrus lemon juice can be proposed in terms of oxygenated terminal of variety natural compounds present in the citrus lemon juice. These natural product molecules have capability of stabilizing agent, capping agent, and chelating agent which played an important role towards the transformation of 1D nanorod morphology into 0D nanoparticles. Moreover, the pH of was changed growth solution due to the presence of ascorbic acid, citric acid, malic acids and also their stabilizing agent, capping agent and chelating agent properties resulted the 0D nanoparticles as can be seen from the Figures 1b. Thus, the compact nature of nanoparticles with uniform electron transfer during the electrochemical reaction can bring obvious role towards the durability of material for long term applications. The citrus lemon juice is naturally rich with acidic compounds, high density of terminated oxygen groups in each molecule for transforming the one dimensional (1D) structure into zero dimensional (0D) structure with typical nanoscale features. The significant variation in the pH of growth solutions with 0.5 mL, 1 mL and 2 mL of lemon juice could play a dynamic role to alter the structure and surface properties of the nanostructured material. From acidic nature of ascorbic acid, malic acid and citric acid, we hereby describe that they have shown influence on the pH of growth solution, consequently the structural transformation and surface modifications were significantly observed. However, the primary use of citrus lemon juice was to alter the pH of growth solution and to induce the significant effect on the structure and surface properties of material. We have also noticed that the relative amount of nanostructured material formation was low when 2 mL of citrus lemon juice was used because of the decreased amount of hydroxyl ions which has slowed down the growth kinetics. From SEM observations, the presence of lemon juice alters significantly the morphology (Figs. 1a and 1b, with and without lemon juice respectively). The rod-like shape is completely lost when lemon juice is used for the catalyst preparation and the outcome catalysts have a powdered disordered structure. Tiny particles are still detectable, as confirmed by XRD analysis of crystallite size.

The crystalline phase was studied by using powder XRD technique and recorded diffraction patterns of different samples including sample 1, sample 2 and sample 3 are shown in Figure 1d. The diffraction patterns of sample 1 prepared with 0.5mL of citrus lemon juice are shown Supplementary Figure (S1). Various diffraction patterns of three samples of $NiCo_2O_4$ nanostructures showed crystal planes such as 111, 220, 311, 222, 400, 422, 511, 531, 442, 533, 620 and 622 and they were well matched the cubic phase of $NiCo_2O_4$. The measured diffraction patterns of $NiCo_2O_4$ nanostructures were in good agreement with the standard JCPDS card (01-080-1542). Interestingly, the increasing volume of citrus lemon juice has reduced the intensity of many of the diffraction peaks due to variation in the pH of growth solution, suggesting the dynamic role of citrus lemon juice about the alteration of shape of $NiCo_2O_4$ nanostructured material. The sample 2 suggests preferential growth along the 400 direction due its strong reflection intensity and offered favorable crystal orientation for high exposure of catalytic sites and swift charge transfer towards the electrochemical applications. This is the point of difference between sample 2 and pure $NiCo_2O_4$ nanostructures and sample 3. The XRD analysis confirmed only the spinel structure with cubic phase of $NiCo_2O_4$ nanostructures and the preparation of high quality nanostructured material. Moreover, an enhanced peak for 620 crystal plane of $NiCo_2O_4$ nanostructures in case of (sample 3) is indicating the preferential growth along this direction and it might change the crystal geometry of $NiCo_2O_4$ nanostructures that could not favor the electrocatalytic activity. The average crystallite size was calculated by Scherrer equation and the calculated values are given in Table 1. It is obvious that 1 mL and 2 mL of lemon juice did not bring substantial influence on the average crystallite size of pure $NiCo_2O_4$ nanostructures and 1 mL (sample 2) and 2 mL of lemon juice (sample 3). A slight increase on average crystallite size is recorded in sample 3.

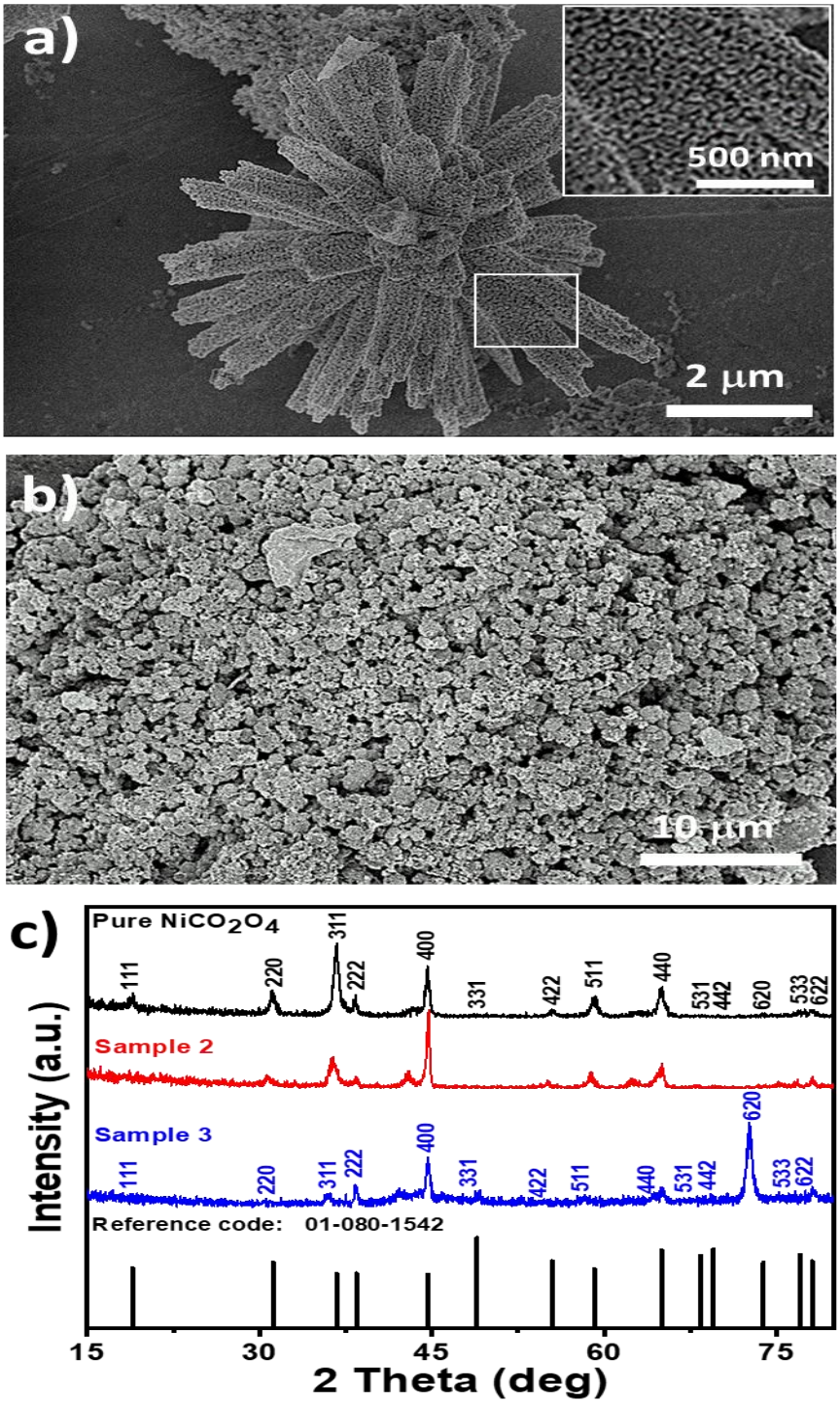

Figure 1: Distinctive SEM images at different magnifications of (a) pristine $NiCo_2O_4$ nanostructures, (b) $NiCo_2O_4$ nanostructures prepared with 1 mL (sample 2) and (c) XRD patterns of pristine $NiCo_2O_4$ nanostructures, (b, c) $NiCo_2O_4$ nanostructures prepared with 1 mL (sample 2), and 2 mL of lemon juice (sample 3).

To have deeper insight on the chemical states of metallic ions and surface vacancies about the pure and citrus lemon juice assisted $NiCo_2O_4$ samples, XPS analysis was performed as shown in Figure 2a. The photoelectron contributions for Co $2p_{3/2}$ signal in the pure $NiCo_2O_4$ sample were observed at 779.5 (Co^{3+}), 781.4 (Co^{2+}), 784.2 (Satellite) and 788.9 (Satellite) eV which is in good agreement with the reported works [44-46]. Similarly, the Ni $2p_{3/2}$ contributions were located at different binding energies such as 854.0 (Ni^{2+}), 855.7 (Ni^{3+}), 857.0 (Ni-OH) and 861.1 (satellite) eV [47]. The relative ratio of Ni^{2+}/Ni^{3+} ions and Co^{2+}/Co^{3+} ions in the pure sample was found to be 1.13 and 0.44 respectively. For the citrus lemon juice assisted $NiCo_2O_4$ nanostructures, the highly resolved spectrum of Co $2p_{3/2}$ was also fitted, the corresponding peaks of Co^{3+} and Co $^{2+}$ were found at binding energies of 779.3, and 781.1 eV, respectively, as shown in Figure 2 [48]. For the Ni $2p_{3/2}$ signal, the fitting showed the contributions at various binding energies 854.0 (Ni^{2+}), 855.7 (Ni^{3+}), 856.1 (Ni-OH) and 860.8 (satellite). The relative ratio of Ni^{2+}/Ni^{3+} ions and Co^{2+}/Co^{3+} ions for citrus lemon juice assisted $NiCo_2O_4$ sample was approximately 1.18 and 0.66, respectively. It is indicating a greater proportion of reduced species on the surface of citrus lemon juice assisted $NiCo_2O_4$ sample compare to pure $NiCo_2O_4$ sample. Moreover, Ni/Co ratio pure $NiCo_2O_4$ sample was changed from 1.02 to 1.37 in case of $NiCo_2O_4$ sample grown with citrus lemon juice. In this regard, the XPS analysis revealed that pure $NiCo_2O_4$ sample and citrus lemon juice assisted $NiCo_2O_4$ sample reveal the coexistence of Ni^{2+}/Ni^{3+} ions and Co^{2+}/Co^{3+} ions on their surface and the presented results are strongly supported by the reported work [49]. Finally, the O 1*s* spectra for the pure $NiCo_2O_4$ sample and citrus lemon juice assisted $NiCo_2O_4$ sample show three essential contributions at ca. 529.5 eV, 531.15 eV, 532.6 eV due to O_{Lat}, O_{Sur}, O_{Che}, respectively. O_{Lat} refers to lattice oxygen in the metal–oxygen structure, O_{Sur} is usually assigned to surface defects and oxygen vacancies, and O_{Che} is assigned to chemisorbed oxygen as revealed by previous studies [44]. By quantifying the different oxygen species in both samples, the O_{Sur}/O_{Lat} ratio changes from 0.52 to 0.76 from pure to citrus lemon juice based sample, indicating that there is a greater proportion of surface species in the latter that could be playing an important role in the OER reaction.

The morphology, crystalline and chemical composition investigations of pristine and citrus lemon juice assisted $NiCo_2O_4$ samples were performed through scanning transmission electron

microscopy (STEM) coupled with energy dispersive X-ray spectroscopy (EDXS), high resolution transmission electron microscopy (HRTEM) and selective area electron diffraction (SAED). The pristine $NiCo_2O_4$ sample is mainly composed of particles of diameter between 20 and 80 nm assembled in nanorod-like structure (Figures 2b, 2d), while citrus lemon juice assisted $NiCo_2O_4$ is composed of aggregates of nanoparticles of less than 20 nm (Figures 2c, 2h). Similar morphological features were observed during SEM analysis. The aggregation of nanoparticles (sample 2) could be ascribed to the collective attraction between nanoparticles through chemical interactions or Vander Waals forces. EDXS experiments confirm the presence of Ni, Co, and O for both samples, without any impurities (Figures 2 d-k). SAED patterns of pure $NiCo_2O_4$ and citrus lemon juice assisted $NiCo_2O_4$ (Figure S2) present rings at 4.7, 2.9, 2.4 and 2.0 Å, corresponding to the Fd-3m cubic structure of $NiCo_2O_4$ (a = 8.1 Å), as found on XRD experiments. The overall observations on both samples suggest that citrus lemon juice has mainly a role in transforming 1D nanorod of pure $NiCo_2O_4$ into 0D nanoparticles.

For better view of structural information, various TEM images were shown (Figure S3), suggesting the effect of citrus lemon juice on the morphology compared to the material prepared without the citrus lemon juice. The TEM analysis confirms the results from SEM: addition of citrus lemon juice inhibits the formation of a rod-shaped structure of self-assembled nanoparticles, and originates a homogeneous distribution of tiny nanoparticles, roughly hierarchically clustered in sub-micrometer sized spheres. Also, the d-spacing were calculated by using HRTEM micrographs of citrus lemon juice assisted juice $NiCo_2O_4$ and pure $NiCo_2O_4$ as shown in Figure S4.

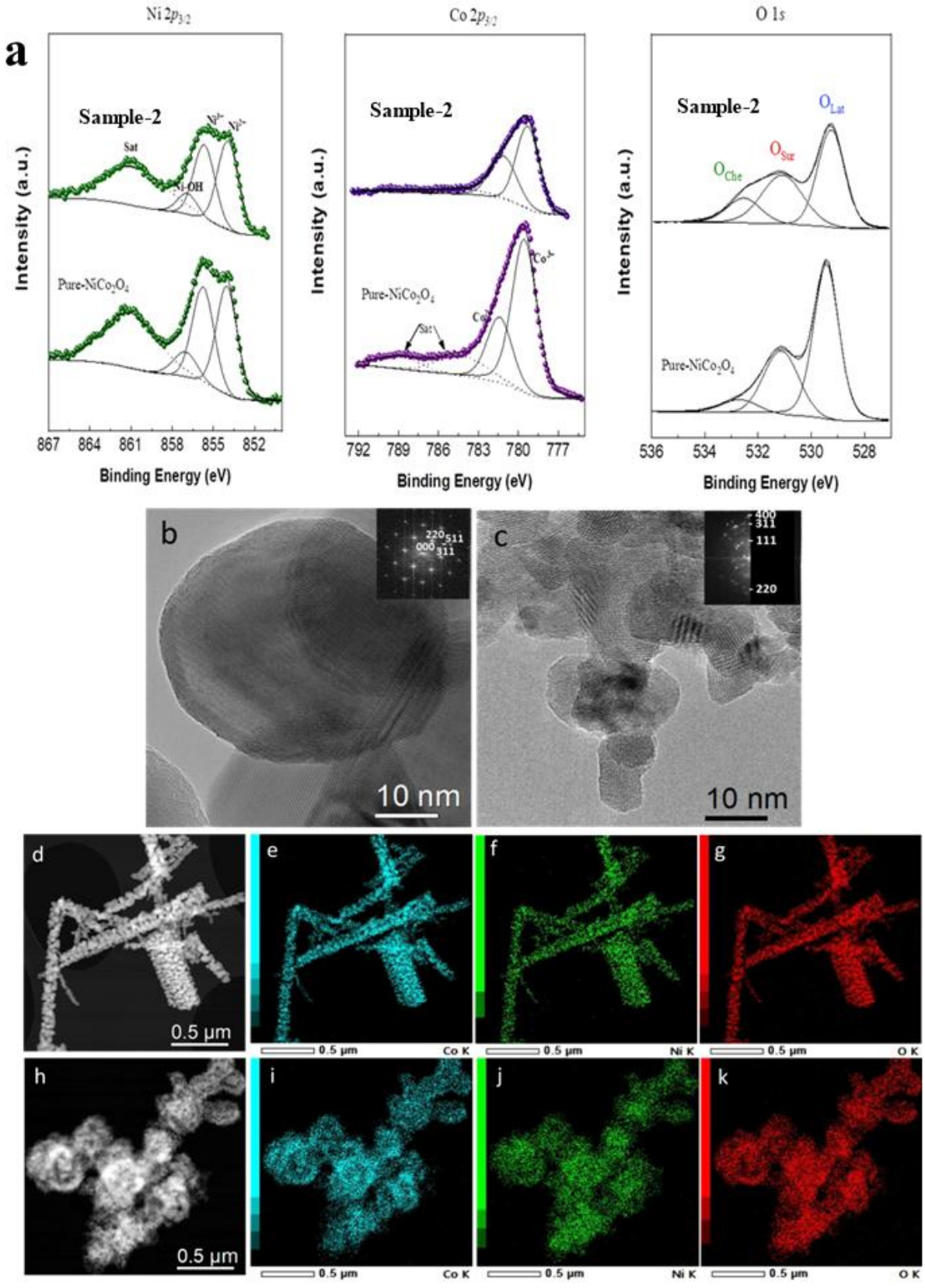
a
Ni 2p3/2
Co 2p3/2
O 1s
Sample-2
Sat
Ni-OH
Pure-NiCo2O4
Intensity (a.u.)
Binding Energy (eV)
867 864 861 858 855 852
792 789 786 783 780 777
536 534 532 530 528
OLat
OSur
OChe
b
c
10 nm
220
511
000
311
400
111
d
e
f
g
h
i
j
k
0.5 μm
Co K
Ni K
O K

Figure 2: Ni $2p_{3/2}$, Co $2p_{3/2}$ and O 1*s* spectra of pure $NiCo_2O_4$ and $NiCo_2O_4$ nanostructures grown with citrus lemon juice with 1 mL (Sample 2) (a). HRTEM micrographs with corresponding Fast Fourier Transform (FFT) (insert of Figures) of pure $NiCo_2O_4$ (b) and citrus lemon juice assisted grown $NiCo_2O_4$ nanostructures (c). STEM High Angle Annular Dark Field (HAADF) of pure $NiCo_2O_4$ (d) and citrus lemon juice assisted grown $NiCo_2O_4$ nanostructures (h) and corresponding X-maps of cobalt (e,i), nickel (f,j) and oxygen (g,k).

3.2. Electrochemical performance evaluation of $NiCo_2O_4$ nanostructures for energy storage applications

Three newly prepared samples of $NiCo_2O_4$ nanostructures including such as (sample 1, sample 2, Sample 3) and pure $NiCo_2O_4$ nanostructures as reference material to understand the role of citrus lemon juice towards tuning the electrocatalytic behavior of materials. The electrochemical performance was evaluated towards the development of SCs. The prepared nanostructured $NiCo_2O_4$ materials were characterized by cyclic voltammetry (CV) and galvanostatic charge-discharge (GCD) curves as shown in Figure 3. Both CV and GCD curves were measured with three electrode cell set up under electrolytic environment of 3.0M KOH aqueous solution as shown in Figure 3(a-f). The CV characterization described the behavior of three materials with pronounced redox behavior at various scan rates ranging from 10-60 mV/s as shown in Figure 3a-c. The area of each curve was enhanced with increasing scan rate. Moreover, the shape of CV curves did not alter with increasing scan rate, suggesting the prepared materials could deliver superior electrochemical performance. The capacitance from CV was observed higher for sample 2 compared to the sample 3 and pure $NiCo_2O_4$ nanostructures at low scan rate. Beside this, GCD curves for these materials were measured at different current densities such as 0.8 to 0.94 Ag^{-1} and their corresponding electrochemical behavior is shown in Figure 3d-f. It is obvious that the sample 2 is exhibiting the longest discharge time in comparison to sample 3 and pure $NiCo_2O_4$ nanostructures as enclosed in Figure 3e. Furthermore, the specific capacitance (C_s) values were calculated at 0.8 Ag^{-1} for the sample 2, sample 3 and pure $NiCo_2O_4$ nanostructures which were found in the order of 358 Fg^{-1}, 163 Fg^{-1}, and 117 Fg^{-1} respectively as shown in Figure 4a. The cyclic stability was also measured at 0.8 Ag^{-1} for three samples and corresponding retention efficiency of C_s were found in the order 100-94%, 108-83%, 90-61%, for sample 2, sample 3 and pure sample, respectively as show in Figure 4b. After 900 cycles, the retention capacitance was

found highest for the sample 1. It is verified that the sample 2 exhibited enhanced cyclic stability with highest retention; hence it could be considered as an optimized electrode material for the development of real energy storage devices. The columbic efficiency for the sample 2, sample 3 and pure sample was observed in the order of 70%, 64%, and 43% respectively as shown in Figure 4c. The energy density was also estimated at 0.8 Ag^{-1} for sample 2, sample 3 and pure sample of $NiCo_2O_4$ nanostructures in the series of 7.96 Wh kg^{-1}, 3.57 Wh kg^{-1}, and 2.47 Wh kg^{-1} respectively. The power densities were also calculated for the sample 2, sample 3 and pure $NiCo_2O_4$ nanostructures with corresponding values of 160.00 KW/Kg, 158.80 KW/Kg, and 156.00 KW/Kg respectively as shown in Figure 4d-f. The evaluated electrochemical activity of as prepared $NiCo_2O_4$ nanostructures (sample 2), (sample 2), and pure $NiCo_2O_4$ nanostructures for the SCs is shown in Table (S3).

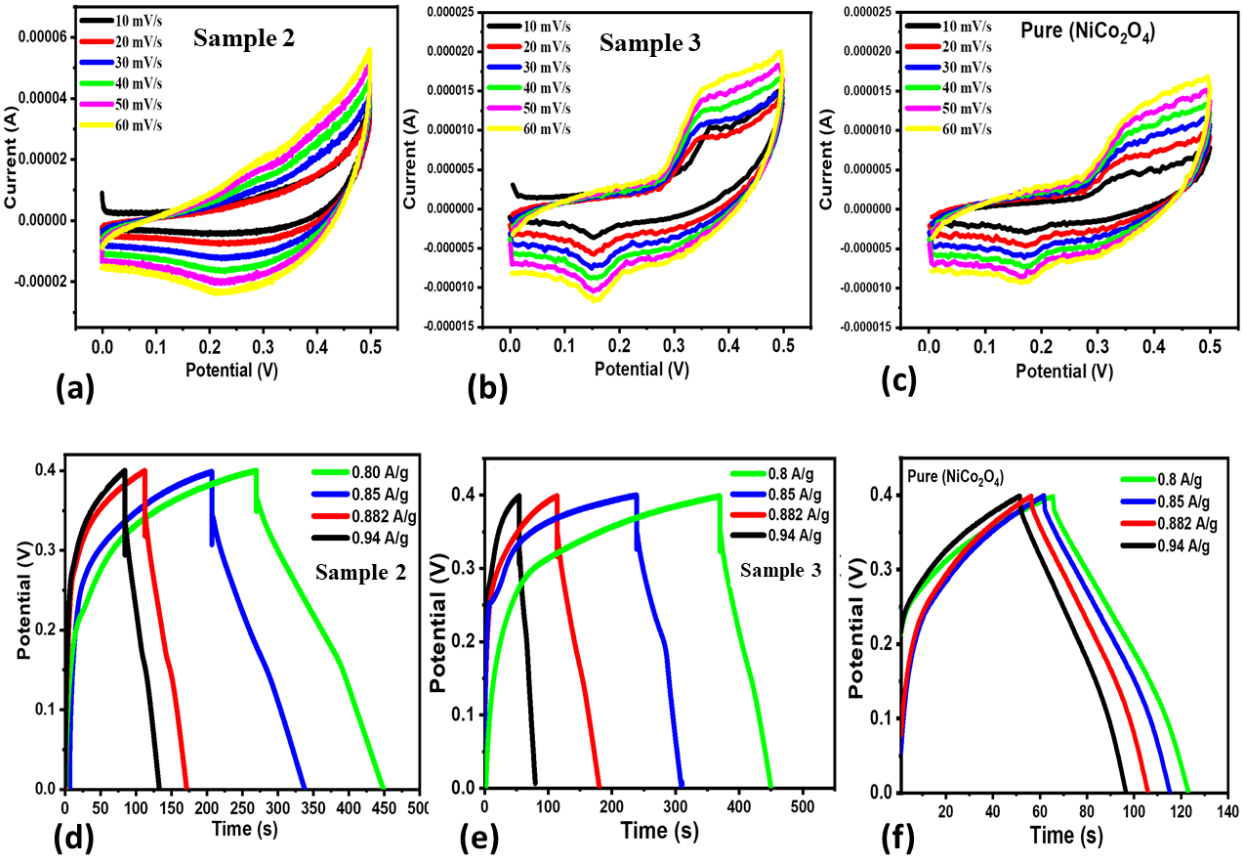

Figure 3: (a-c) Various CV curves at different scan rates for $NiCo_2O_4$ (sample 2), $NiCo_2O_4$ (sample 3), pure $NiCo_2O_4$ nanostructure, in 3.0M KOH aqueous electrolytic solution. (d-f)

Corresponding GCD curves at various current densities of 0.8, 0.85, 0.88, and 0.94 Ag^{-1} performed in 3.0M KOH solution.

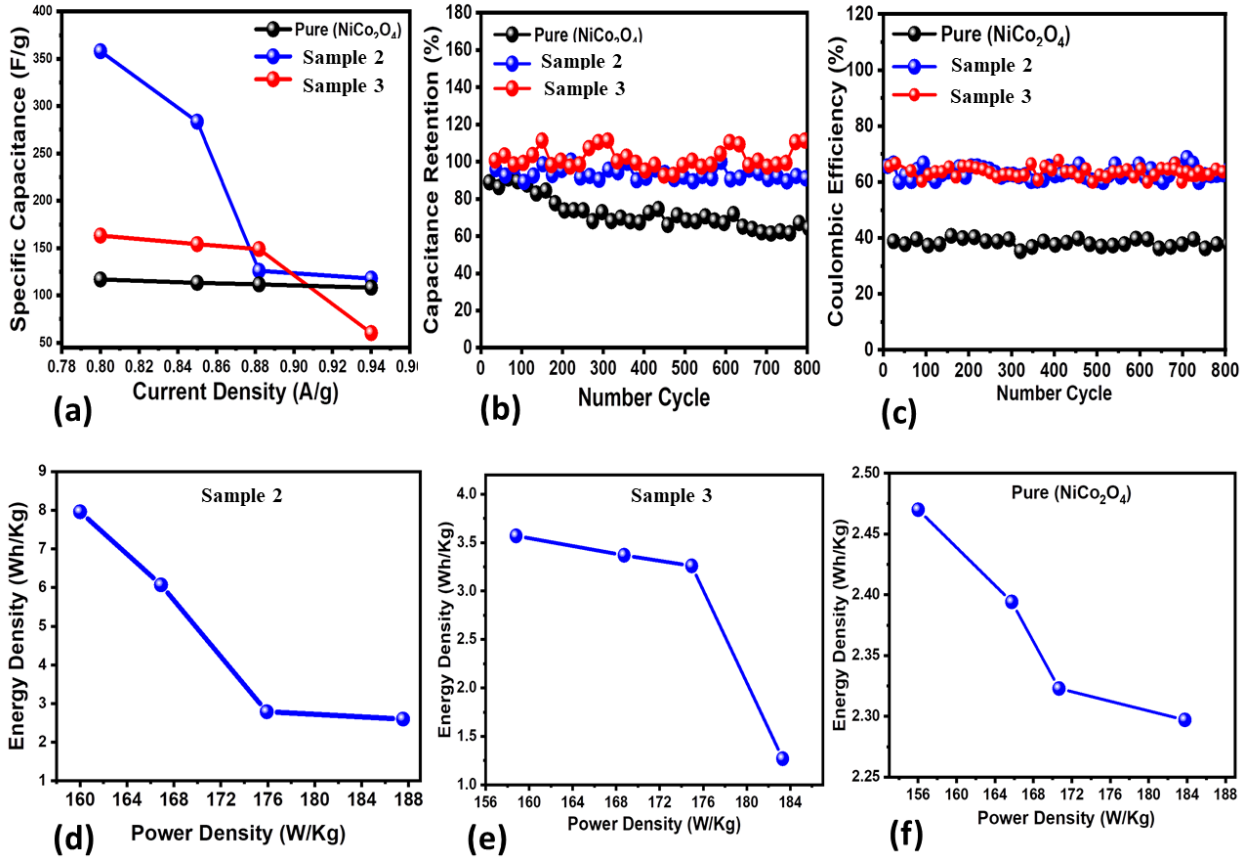

Figure 4: (a) specific capacitance (Cs) of pure $NiCo_2O_4$ nanostructure, (sample 2) and (sample 3) from GCD curves, (b) percentage retention specific capacitance of pure $NiCo_2O_4$ nanostructure (sample 2), (sample 3) from cycling stability of GCD curves, c) columbic efficiency of pure $NiCo_2O_4$ nanostructure, (sample 2) and (sample 3) from cycling stability of GCD curves, (d-f) corresponding energy density of pure $NiCo_2O_4$ nanostructure, (sample 2) and (sample 3).

For three electrode supercapacitor application, the cyclic stability for the sample 1 is either equal or higher to many of the recently reported electrode materials as given in Supplementary Table (S3). Many of the materials reported in the Supplementary Table (S3) are complex in nature and involving hybrid systems which apparently have excellent performance. However our presented

material synthesis approach is facile, low cost, ecofriendly and environment friendly and it has comparable of specific capacitance to the previous studies, hence offering an alternative material with promising green synthetic strategy for the scale up synthesis of nanostructured materials. The citrus lemon juice has changed the pH of growth solution and it has influenced on the structural transformation, surface modification and the exposed the favorable crystal facets for the enhanced electrochemical performance. The performance of our material can be enhanced compare to the existing literature on the supercapacitor application by high loading of proposed material onto large surface area electrode. Despite the use of low current density of 0.8 Ag^{-1} and narrow potential window, we have obtained the considerable high energy density and specific capacitance using newly prepared $NiCo_2O_4$ nanostructures (sample 2).

Before to the development of two electrode asymmetric supercapacitor device, we have evaluated the supercapacitor properties of activated carbon using three electrode cell configuration and the measured performance is enclosed in Supplementary Figure (S5). First GCD curves were obtained at various current densities of 0.8, 0.85, 0.88 and 0.94 Ag^{-1}, then specific capacitance of 247 F/g and energy density of 5.47 Wh/Kg were calculated as shown in Supplementary (S5). The analyzed results if GCD curves indicated the poor performance of activated carbon (AC).

The practical aspects of $NiCo_2O_4$ nanostructures (sample 2), was also studied by developing asymmetric supercapacitor (ASC) using anode of $NiCo_2O_4$ nanostructures (sample 2), and activated carbon as cathode electrode in aqueous 3.0M KOH solution. The ASC was represented by ($NiCo_2O_4$ Sample 2//AC ASC).

The CV curves of ($NiCo_2O_4$ Sample 2) and for AC for the potential range of -0.2 to 1.5 V are shown in Supplementary Figure (S5) and it was assumed that the operating potential window of ($NiCo_2O_4$ Sample 2//AC ASC) could be enlarged to 1.45 V and the potential window was selected according to published work [50-54]. Further increasing the potential range could cause the H_2/O_2 evolution reaction as previously reported [50, 51]. Hence, the optimum operational potential window was kept approximately to 1.45 V to examine the electrochemical activity of asymmetric device ($NiCo_2O_4$ Sample 2//AC ASC) and the corresponding CV curves are enclosed in Supplementary Figure (S6). The CV results have revealed the overall phenomenon of capacitance of ($NiCo_2O_4$ Sample 2//AC ASC) was extracted from double-layer capacitance and battery like aspects of newly prepared spinel bimetallic oxide material. From CV curves, it is

clear that there is no change of shape of CV, indicating the swift charge-discharge features of ($NiCo_2O_4$ Sample 2//AC ASC) device. The corresponding GCD curves of ($NiCo_2O_4$ Sample 2//AC ASC) were also measured as shown in Supplementary Figure (S6) for the current density range of 0.8 to 0.94 Ag^{-1} and derived different calculation values of ASC characterization are enclosed in Supplementary Figure (S6). The capacitance retention for the 900 cycles was found around 64-52%, which is still far better than many of the reported works on bimetallic oxides in the literature as shown in Supplementary Figure (S6). The specific capacitance C_s at $0.8Ag^{-1}$ was calculated as 1519 Fg^{-1} even at a $0.94Ag^{-1}$ specific capacitance was found high like 1459 Fg^{-1} as shown in Supplementary Figure (S6). The estimated energy density of 33.08 Wh kg^{-1} is relatively higher than the reported works with a power density of 633 W/kg, confirming the significant advancement in the field of ASC devices as shown in Supplementary Figure (S6). The columbic efficiency of 100-84% was also an excellent for the presented ASC system as shown in Supplementary Figure (S6). A power density of 633 W/kg is reflecting that the ($NiCo_2O_4$ Sample 2//AC ASC) can maintain the energy density of 33.1 Wh kg^{-1}, suggesting that these values are still impressive compared to the already existing $NiCo_2O_4$ based ASCs systems such as composite system of $NiCo_2O_4$@MnO_2 hybrid//AC (an energy density of 37.8 Wh kg^{-1} at power density 187.5 W kg^{-1}) [52], N–doped carbon–coated $NiCo_2O_4$//AC (29.4 Wh kg^{-1} at the power density of 349 W kg^{-1}) [55],

HDC@$NiCo_2O_4$@PPy//HDC@$NiCo_2O_4$@PPy (17.5 Wh kg^{-1} at the power density of 500 W kg^{-1}) [50], $NiCo_2O_4$ microspheres//AC (45.3 Wh kg^{-1} at the power density of 533.3 W kg^{-1}) [56], $NiCo_2O_4$/NGN/CNTs//NGN/CNTs (42.7 Wh kg^{-1} at the power density of 775 W kg^{-1}) [51], and $NiCo_2O_4$@Co–Fe LDH//AC (28.94 Wh kg^{-1} at the power density of 950 W kg^{-1}) [52]. Beside $NiCo_2O_4$ based ASCs devices, the previously reported ASCs based on other materials have either inferior or equal performance to the presented ($NiCo_2O_4$ Sample 2//AC ASC) such as CuS hollow micro flowers//AC (15.97 Wh kg^{-1} at a power density of 185.4 W kg^{-1}) [57], and Ni_3Se_2 3D HMNN//AC (38.4 Wh kg^{-1} at a power density of 794.5 W kg^{-1}) [58]. For the simplicity, the observed performance of ASC is provided in the Table (S3).

3.3. Oxygen evolution reaction performance evaluation of various citrus lemon juice **assisted $NiCo_2O_4$ nanostructures**

Electrochemical performance of $NiCo_2O_4$ nanostructures was studied for OER half-cell water splitting in 1.0M KOH aqueous solution using three electrode cell configuration. For this

characterization, LSV was used for the pure $NiCo_2O_4$ and lemon juice assisted $NiCo_2O_4$ nanostructures (sample1, sample 2, sample 3) at sweeping scan rate of 2 mV/s and corresponding iR corrected polarization curves are enclosed in Figure 5a. The performance of these newly prepared materials of $NiCo_2O_4$ was also compared with the reference noble metal (RuO_2) electrocatalyst as shown in Figure 5a. The overpotential for $NiCo_2O_4$ nanostructures grown with 1 mL of citrus lemon juice was found to be 250 mV at 10 $mAcm^{-2}$, which is smaller than pure and 2mL citrus lemon juice assisted $NiCo_2O_4$ nanostructures. An overpotential of 270 mV at 10 $mAcm^{-2}$ was recorded for the pure and 2 mL assisted $NiCo_2O_4$ nanostructures as shows in Figure 5a. Whereas the sample 1 has shown relatively better performance compare to the pure $NiCo_2O_4$ nanostructures with a low overpotential of 280 mV at 10 $mAcm^{-2}$. However, 1 mL of citrus lemon juice drastically changed the OER activity of $NiCo_2O_4$ nanostructures with lower overpotential compare to sample 1, sample 2 and pure $NiCo_2O_4$ nanostructures. The pure $NiCo_2O_4$ nanostructures have shown the limiting performance owing to its low density of active sites and poor electron transfer capacity. An addition of 2 mL of citrus lemon juice supplied high concentration of reducing agents which significantly enabled the surface with limited number of active sites and charge transport of the material, hence poor performance $NiCo_2O_4$ nanostructures was observed compared to the sample 2. The linear region of LSV polarization curves was used to assess the reaction kinetics and the estimated Tafel plots are given in Figure 5b. Significantly, the Tafel slope of $NiCo_2O_4$ nanostructures grown with 1 mL was as low as 98 $mVdec^{-1}$ which is lower compare to pure and 2 mL assisted $NiCo_2O_4$ nanostructured materials (105 $mVdec^{-1}$, and 112 $mVdec^{-1}$ respectively). The Tafel slope of sample 1 was estimated about 107 $mVdec^{-1}$. The Tafel analysis revealed that the $NiCo_2O_4$ nanostructures grown with 1 mL of citrus lemon juice has speedy OER kinetics due to favorable catalytic surface properties. Stability of 1 mL assisted $NiCo_2O_4$ nanomaterial was also studied in 1.0M KOH using LSV polarization curves before and after the durability measurements as shown in Figure 5c. It was noticed that the durability test for 40 hour did not alter the onset potential, overpotential and current density, suggesting the high stability and compatibility of material with the GCE. Durability is an important parameter to examine the activity of nonprecious catalyst; hence chronopotentiometry was used to describe the electro catalytic durability of $NiCo_2O_4$ nanostructures prepared with 1 mL of citrus lemon juice as shown in Figure 5d. There was negligible overpotential drop at constant 20 $mAcm^{-2}$ for the period of 40 hours, confirming the durability of material for a significant period of OER

operation. The $NiCo_2O_4$ nanostructures have been found stable under 1.0M KOH alkaline conditions and they are strongly supported by the reported works elsewhere. It has been observed that the electrochemical active surface area (ECSA) is directly connected to the double layer capacitance (Cdl) of an electrocatalyst [59], and known as a crucial parameter to assess the amount of active sites on the surface of catalyst and they have to be involved in the electrochemical reaction. For this purpose, cyclic voltammetry (CV) curves were measured with non-Faradic regions to calculate the Cdl as shown in Supplementary Figure (S7). The Cdl values were obtained by plotting the difference of anodic and cathodic current densities at 0.2V versus RHE against different scan rates [60]. The Cdl is considered as a half value of slope achieved after linear fitting and ECSA could be measured by using equation of ECSA= Cdl/C_s. The C_s is a constant value related to nature of electrode material surface which is found to be 40 $mFcm^{-2}$ in 1.0M KOH as previously reported [61]. The measured values of ECSA for three nanostructures of $NiCo_2O_4$ nanostructures (sample 2, sample 3) and pure sample were in the order, 15.2 μFcm^{-2}, 8.2 μFcm^{-2}, and 6.3 μFcm^{-2} respectively. The ECSA calculations revealed that the $NiCo_2O_4$ nanostructures (sample 2) with highest value is describing the predominant contributing factor towards faster OER activity. Furthermore, the charge transfer resistance rate was also evaluated for the $NiCo_2O_4$ nanostructures prepared with and without citrus lemon juice during OER operation using electrochemical impedance spectroscopy (EIS) as shown in Figure 5e. Bode plots obtained from EIS data at different sweeping frequencies are shown in Figure 5f. The Nyquist plot with higher frequency region has shown the information about the porosity of electrode film whereas in the low frequency region the sub circuit is associated with the charge transfer resistance [62]. The fitted circuit has provided the charge transfer resistance values for three $NiCo_2O_4$ nanostructures (sample 2, sample 3 and pure) are in order 165 Ω, 547 Ω and 968 Ω respectively and these values are provided in the Table (S6). The charge transfer resistance of low value for the sample 2, further supported its OER performance in 1.0M KOH aqueous solution. The XRD results of sample 2 has revealed that the preferred crystal orientation along the 400 crystal plane with high intensity has shown desirable crystal orientation for the exposure of high surface catalytic sites, consequently fast charge transport has been shown at the interface of electrode and electrolyte. The HRTEM study has shown that $NiCo_2O_4$ (sample 2) is composed of nanoparticles of less than 20 nm and exhibited a large surface area. Therefore, a low nanoscale dimension of less than 20 nm for the sample 2 offered frequent contact with electrolyte, thus

efficient electrochemical performance was observed. The SAED patterns of lemon assisted $NiCo_2O_4$ (sample 2) presents rings at 2.4 and 2.0 Å, indicating small lattice rings and they could be further effectively driven the electrochemical activity of material towards supercapacitor and half-cell OER applications. The improved performance of proposed electrocatalyst from fundamental point of view could be explained in terms of shape transformation of material, variation in the crystal orientation, high surface oxygen vacancies, high active sites, fast charge transfer rate at the interface of electrode and electrolyte favored the electrocatalytic kinetics, high Ni/Co ratio of 1.37 in case of citrus lemon juice assisted $NiCo_2O_4$ sample , and biomimetic features of citrus lemon juice assisted $NiCo_2O_4$ sample supported the high compatibility with glassy carbon electrode. The present study was aimed to understand the fundamental role of structural transformation, creation of defects on the surface, and to alter the crystal orientation during growth process, therefore they together insightfully enhanced the electrochemical performance of $NiCo_2O_4$ nanostructures. These fundamental features of prepared $NiCo_2O_4$ nanostructures of presented study bring an advancement in the development of new generation of electrocatalysts for the energy conversion and storage systems. Furthermore, an enhanced SC and electro catalytic performances of $NiCo_2O_4$ nanostructures (sample 2) were contributed from unique fabrication aspects, such as short range nanoparticles resulted from the unique chemistry of citrus lemon juice has exposed the material at large extent to the electrolytic molecules. The use of biomass packed the nanoparticles avoided the volume changes, hence maintained the mechanical strength, demonstrating the significant cycling stability during SC and OER processes.

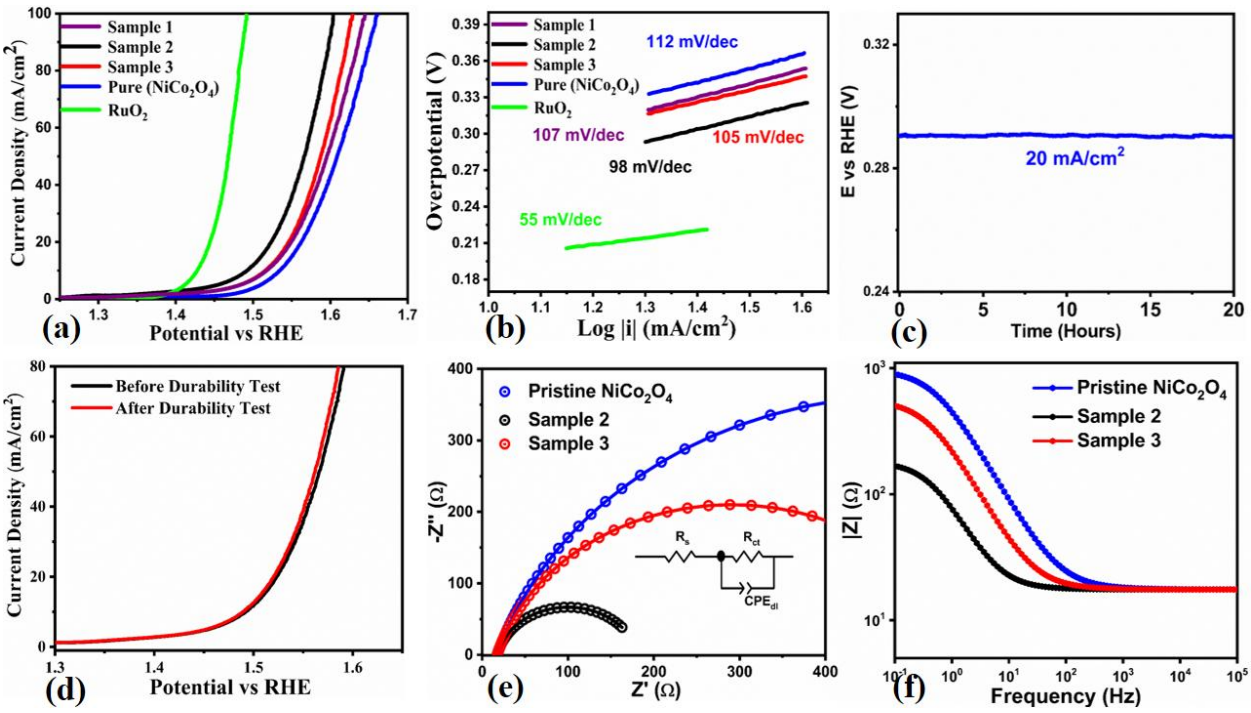

Figure 5: (a) LSV polarization curves at 2 mV/s for pristine $NiCo_2O_4$ nanostructure, $NiCo_2O_4$ (sample 2), $NiCo_2O_4$ (sample 3) and RuO_2 in 1.0M KOH aqueous solution, (b) Corresponding Tafel analysis of pristine $NiCo_2O_4$ nanostructure, $NiCo_2O_4$ (sample 2), $NiCo_2O_4$ (sample 3) and RuO_2, (c) stability of $NiCo_2O_4$ (sample 3) (d) durability for 40 hours at 20 $mAcm^{-2}$, (e) Electrochemical impedance spectroscopy (EIS) Nyquist plots of pristine $NiCo_2O_4$ nanostructure, $NiCo_2O_4$ (sample 2), $NiCo_2O_4$ (sample 3) for frequency range of 100 kHz to 0.1 Hz at an amplitude of 5 mV and onset potential of OER, inset shows the fitted equivalent circuit (f) Corresponded Bode Plots of pristine $NiCo_2O_4$ nanostructure, $NiCo_2O_4$ (sample 2), $NiCo_2O_4$ (sample 3) from same EIS

The OER performance of $NiCo_2O_4$ nanostructures (sample 2) prepared with citrus lemon juice was compared with the previously reported electrocatalyst as given in Table S6. It is shown that activity of $NiCo_2O_4$ nanostructures (sample 2) is superior to many of the catalyst in terms of low overpotential of 250 mV at the same current density and 1.0M KOH aqueous solution, confirming the dynamic role of natural molecules from citrus lemon juice on the enhanced activity towards water splitting. Importantly, the synthetic strategy of presented work is green, used minimum toxic chemicals, low cost, scale up for the synthesis of large quantity of material, ecofriendly and environment friendly. Furthermore, the obtained electrochemical performance is shown bar graph for the better understanding and view as enclosed in Supplementary Figure

S8 (a-d). We report the obtained results in these bar graphs for OER overpotential at 10 and 50 $mAcm^{-2}$, Tafel values, specific capacitance (C_s) and energy density, respectively, for the pristine and citrus lemon juice assisted $NiCo_2O_4$ nanostructures (sample 1, sample 2, sample 3) and RuO_2. For better view, the OER of (sample 1, sample 2, sample 3) and capacitance performance of the pure and citrus lemon juice assisted $NiCo_2O_4$ nanostructures (sample 2, sample 3) are given in Table 2. It is clear that the sample 2 has relatively better electrochemical activity compare to pure and sample 2.

Table 2: Overall performance comparison of the pristine and citrus lemon juice assisted $NiCo_2O_4$ nanostructures (sample 1, sample 2).

Sample ID	**Over potential (mV)@10 $mAcm^{-2}$**	**Tafel Slope ($mVdec^{-1}$)**	**Charge Transfer Resistance (Rct) (Ω)**	**Specific Capacitance (F/g) @ 0.8 A/g**	**Energy Density (Wh/kg) @ 0.8 A/g**	**Power Density (W/kg) @ 0.8 A/g**
Pure ($NiCo_2O_4$)	300	112	968	117	2.47	156
Sample 1	280	107	-	-	-	-
Sample 2	250	98	165	358	7.95	160
Sample 3	280	105	547	163	3.57	159

4. Conclusions

In summary, we have used natural resources of chemical compounds with stabilizing agent, capping agent and chelating properties from citrus lemon juice for the preparation of 0D nanoparticles of $NiCo_2O_4$ using hydrothermal. The structure, chemical composition and crystalline studies were carried out by wide range of analytical techniques. We have observed that 1D nanorod morphology of $NiCo_2O_4$ was successfully transformed into 0D nanoparticles due to change in pH of growth solution, capping agent, stabilizing agent and chelating agent properties of citric acid, malic acid and ascorbic acid during growth process. At the same time, these natural products have tailored surface properties, enhanced electron communication, fast ionic diffusion of electrolyte, swift charge transfer at the interface of electrode and electrolyte.

For this reason, we have noticed an excellent OER reaction at an overpotential of 250mV at 10 $mAcm^{-2}$ with a durability of 40 hours under alkaline conditions. Furthermore, we have also studied the energy storage aspects of $NiCo_2O_4$ material for the development of asymmetric supercapacitor and observed values of specific capacitance (C_s) of 1519.19 Fg^{-1}, and energy density of 33.08 Wh kg^{-1} are highly meritorious. The extended spectrum of electrochemical properties of $NiCo_2O_4$ material, associated with our low cost and facile approach enabled it highly favorable for the development of high performance energy conversion and storage systems in near future.

Acknowledgments

The authors extend their sincere appreciations to Researchers Supporting Project number (RSP2023R79), King Saud University, Riyadh, Saudi Arabia, for partial funding of this work. B.V. and E.M would like to also thank the platform "Microscopies, Microprobes and Metallography (3M)" at the Institut Jean Lamour (IJL, Nancy, France) for TEM and SEM facilities. A.V. acknowledges the Kempe Foundation and the Knut och Alice Wallenberg Foundation for financial support.

Author contribution

Shusheel Kumar, carried out material synthesis and water catalysis

Aneela Tahira, did XRD analysis

Adeel Liaquat Bhatti, did impedance measurement

Muhammad Ali Bhatti[d], did OER analysis

Riaz Hussain Mari[a], did partial supervision

Nek Muhammad Shaikh, did partial supervision

Muhammad Yameen Solangi, did ECSA and Tafel analysis

Ayman Nafady, did preview the obtained results

Mélanie Emo, did TEM analysis

Brigitte Vigolo, did SEM analysis and proofread the paper

Antonia Infantes-Molina, did XPS analysis and proofread the paper

Alberto Vomiero, did the final preview and proofread the paper

Zafar Hussain Ibupoto, did supervision and wrote first draft of manuscript

Conflict of Interest

Authors declare no conflict of interest in this research work

5. References

[1] J. Yan, Q. Wang , T. Wei and Z. Fan, Adv Energy Mater, 2014, 21, 1300816–1300859.

[2] K. S. Poonam, A. Arora, and S. K. Tripathi, J. Energy Storage 2019, 21, 801.

[3] J.Gou , Y. Du ,S. Xie ,Y. Liu , X. Kong, Inter J Hydrogen Energ 2019, 44, 27214–27223.

[4] V.Raman ,N.V. Mohan ,B. Balakrishnan ,R. Rajmohan ,V. Rajangam ,A. Selvaraj ,H.J. Kim. Ionics 2020, 26, 345–354.

[5] F. Wang, Y. Li , Z.Cheng ,K. Xu , X.Zhan ,Z. Wang. Phys Chem Chem Phys 2014, 16, 12214–12220.

[6] J.Gou ,S. Xie ,B. Xu, Ionics, 2020, 26, 337–344.

[7] L. Liu, H. Zhang, J. Yang, Y. Mu, Y. Wang, J. Mater. Chem. 2015, 3, 22393–22403.

[8] H. Fu, Y. Liu, L. Chen, Y. Shi, W. Kong, J. Hou, F. Yu, T. Wei, H. Wang, X. Guo, Electrochim. Acta 2019, 296, 719–729.

[9] T. Liu, P. Diao, Nano Res. 2020, 13, 3299–3309.

[10] L. Kumar, M. Chauhan, P.K. Boruah, M.R. Das, S.A. Hashmi, S. Deka, ACS Appl. Energy Mater 2020, 3, 6793–6804.

[11] Y. Zhu, X. Ji, Z. Wu, W. Song, H. Hou, Z. Wu, X. He, Q. Chen, C.E. Banks, J. Power Sources 2014, 267, 888–900.

[12] X. Gao, H. Zhang, Q. Li, X. Yu, Z. Hong, X. Zhang, C. Liang, Z. Lin, Angew. Chem. Int. 2016, 55, 6290–6294.

[13] A. Mondal, S. Maiti, S. Mahanty, A. B. Panda, J. Mater. Chem. 2017, 5, 23853-23862.

[14] L. Fang, Z. Jiang, H. Xu, L. Liu, Y. guan, X. Gu, Y. Wang, J. Catal. 2018, 357, 238–246.

[15] X. Lv, Y. Zhu, H. Jiang, X. Yang, Y. Liu, Y. Su, J. Huang, Y. Yao, C. Li, Dalton Trans.2015, 44, 4148–4154.

[16] S. E. Hosseini and M. A. Wahid, *International Journal of Energy Research* 2020, 44, 4110-4131.

[17] F. Perera, International journal of environmental research and public health 2018, *15*, 16-27.

[18] R. M. Elavarasan ,IEEE Access 2020, *8*, 74432-74457.

[19] A. Olabi and M. A. Abdelkareem, Renewable and Sustainable Energy Reviews 2022,*158*, 112111.

[20] D. Gielen, F. Boshell, D. Saygin, M. D. Bazilian, N. Wagner, and R. Gorini, Energy Strategy Reviews 2019,*24*, 38-50.

[21] Q. Wang and K. Domen, Chemical Reviews 2019, 120, 919-985.

[22] M.-I. Jamesh and X. Sun, Journal of Power Sources 2018,*400*, 31-68.

[23] Q. Zhang and J. Guan, Journal of Power Sources 2020, 471, 2284-94.

[24] L. M. Cao , L. Li, P. Wang, Q. Shao ,Advanced science 2018, *33*, 18009-20.

[25] N.-T. Suen, S.-F. Hung, Q. Quan, N. Zhang, Y.-J. Xu, and H. M. Chen, Chemical Society Reviews 2017, *46*, 337-365.

[26] Z. Chen, X. Duan, W. Wei, S. Wang, and B.-J. Ni, Nano Energy 2020,*78*, 1052-72.

[27] E. Fabbri, A. Habereder, K. Waltar, R. Kötz, and T. J. Schmidt, Catalysis Science & Technolog 2014, *4*, 3800-3821.

[28]. Y. Matsumoto and E. Sato, Materials chemistry and physics 1986, *14*, 397-426.

[29]. Q. Liang, J. Chen, F. Wang, and Y. Li, Coordination Chemistry Reviews 2020, *424*, 2134-88.

[30]. Z. Lu , L. Li, P. Wang, Q. Shao ,Nature communications 2014, *5*, 1-7.

[31]. L. Gao, X. Cui, Z. Wang, C.D. Sewell, Z. Li, S. Liang, M. Zhang, J. Li, Y. Hu and Z. Lin, *Proceedings of the National Academy of Sciences*, 2021, *118*, p.e2023421118.

[32]. L. Gao, X. Cui, C.D. Sewell, J. Li and Z. Lin *Chemical Society Reviews*, 2021, *50*, 8428-8469.

[33]. V. Vij, S. Sultan, A. M. Harzandi, A. Meena, J. N. Tiwari, W. G. Lee, T. Yoon, and K. S. Kim, 2017. *Acs Catalysis*, 2017, *7*, 7196-7225.

[34]. D. Khalafallah, M. Zhi, and Z. Hong, ChemCatChem 2021, *13*, 81-110.

[35]. M. Kaur, P. Chand, H. Anand, Inorganic Chemistry Communications 2021, 134, 1089-96.

[36]. A. Sasmal, and A. K. Nayak, Journal of Energy Storage 2023, 58, 106342.

[37]. O. C. Pore, A. V. Fulari, N. B. Velhal, V. G. Parale, H. H. Park, R. V. Shejwal, V. J. Fulari, and G. M. Lohar, Materials Science in Semiconductor Processing 2021, 134, 105980.

[38]. A. K. Yedluri, & H. J. Kim, RSC advances, 2019, 9, 1115-1122.

[39]. M. Kaur, P. Chand & H. Anand, Inorganic Chemistry Communications, 2021, 134, 108996.

[40]. A. G. Solangi, T. Pirzada, A. A. Shah, I. A.Halepoto, A. S. Chang, Z. Solangi, M.Y.Solangi, Journal of the Chinese Chemical Society, 2022, 69, 1608-1618.

[41]. P. M. Shafi, N. Joseph, R. Karthik, J.-J. Shim, A. C. Bose, and V. Ganesh, *Microchemical Journal* 2021, *164*, 1059-45.

[42]. R. V. Poonguzhali , L. Li, P. Wang, Q. Shao ,Ceramics International 2021, *47*, 23110-23115.

[43]. M. Klimek-Szczykutowicz, A. Szopa, and H. Ekiert, *Plants* 2020, 9, 119.

[44]. A. J. Laghari, *Z.Ibhupoto, A.L.Bhatti, International Journal of Hydrogen Energy* 2022, 48, 482-95.

[45]. A. L. Bhatti ,*Z.Ibhupoto, A.Tahira,U.Aftab, Electrochimica Acta* 2021, *398*, 13933-38.

[46]. U. Aftab, A. J. Laghari, *Z.Ibhupoto, A.L.Bhatti, Catalysis Science & Technology* 2019, *9*, 6274-6284.

[47]. Y.-T. Lu, Y.-J. Chien, C.-F. Liu, T.-H. You, and C.-C. Hu, Journal of Materials Chemistry A 2017, 5, 21016-21026.

[48]. Y.L. Tong, L. Xing, M. Z. Dai, and X. Wu, *Frontiers in Materials*, 2019, *6*, 233.

[49]. D.Y. Lei, X.D. Li, M.K. Seo, M.S. Khil, H.Y. Kim, B.S. Kim, Polymer 2017, 132, 31-40.

[50]. J. Pu, J. Wang, X.Q. Jin, F.L. Cui, E. Sheng, Z.H. Wang, Electrochim. Acta 2013, 106, 226-234.

[51]. Y.Q. Wu, X.Y. Chen, P.T. Ji, Q.Q. Zhou, Electrochim. Acta 2011, 56, 7517-7522.

[52]. N. Iqbal, X.F. Wang, A.A. Babar, J.Y. Yu, B. Ding, J. Colloid Interface Sci., 2016, 476, 87-93.

[53]. L. Chang, L. Mai, X. Xu, Q. An, Y. Zhao, D. Wang, and X. Feng, *RSC advances*, 2013, *3*, 1947-1952.

[54]. Z. Xu, J. Ren, Q. Meng, X. Zhang, C. Du, J. Chen, ACS Sustain. Chem. Eng. 2019, 7, 12447–12456.

[55]. L. Liu, H. Zhang, J. Yang, Y. Mu, Y. Wang, J. Mater. Chem. A 2015, 3, 22393–22403.

[56]. Y. Liu, Z. Zhou, S. Zhang, W. Luo, G. Zhang, Appl. Surf. Sci. 2018, 442, 711–719.

[57]. Y. Liu, Q. Xu, R. Wang, Y. Zheng, L. Zhu, Z. Wang, W. Zheng, J. Mater. Chem. 2020, 8, 797–809.

[58]. G. Zhang, Q. Qin, W. Luo, Y. Liu, C. Jin, J. Hao, J. Zhang, W. Zheng, ,Chem. Commun. 2018, 54, 4617–4620.

[59]. Q. Xu, Y. Liu, Z. Tian, Y. Shi, Z. Wang, W. Zheng, Electrochim. Acta, 2021, 385, 1384-29.

[60]. W. Li, X. Gao, D. Xiong, F. Wei, W.G. Song, J. Xu, L. Liu, Adv. Energy Mater. 2017, 7, 16025-79.

[61]. L. Birry, A. Lasia, J. Appl. Electrochem. 2004, 34, 735–749.

[62]. L. Liao, S. Wang, J. Xiao, X. Bian, Y. Zhang, M.D. Scanlon, X. Hu, Y. Tang, B. Liu, H. H. Girault, Energy Environ. Sci. 2014, 7, 387–392.

Supporting Information

Green synthetic route for transforming 1D $NiCo_2O_4$ nanorods into 0D nanoparticles: Advanced approach towards efficient asymmetric supercapacitor and water oxidation

Shusheel Kumar[a], Aneela Tahira[c], Adeel Liaquat Bhatti[a], Muhammad Ali Bhatti[d], Riaz Hussain Mari[a], Nek Muhammad Shaikh[a], Muhammad Yameen Solangi[e], Ayman Nafady[j], Mélanie Emo[f], Brigitte Vigolo[f], Antonia Infantes-Molina[g], Alberto Vomiero[*h,i], Zafar Hussain Ibupoto[*b]

[a]Institute of Physics, University of Sindh Jamshoro, 76080, Sindh Pakistan

[b]Institute of Chemistry, University of Sindh Jamshoro, 76080, Sindh Pakistan

[c]Institute of Chemistry, Shah Abdul Latif University Khairpur Mirs, Sindh, Pakistan

[d]Institute of Environmental Sciences, University of Sindh Jamshoro, 76080, Sindh Pakistan

[e]Mehran University of Engineering and Technology, 7680 Jamshoro, Sindh Pakistan

[f]Université de Lorraine, CNRS, IJL, F-54000 Nancy, France

[g]Department of Inorgnic Chemistry, Crystallography and Mineralogy. (Unidad Asociada al ICP-CSIC), Faculty of Sciences, University of Malaga, Campus de Teatinos, 29071, Malaga, Spain

[h]Department of Engineering Sciences and Mathematics, Division of Material Science, Luleå University of Technology, Luleå, Sweden

[i]Department of Molecular Sciences and Nanosystems, Ca' Foscari University of Venice, Venezia Mestre, Italy

[j]Chemistry Department, College of Science, King Saud University, Riyadh, 11451, Saudi Arabia

*__Corresponding authors__: Alberto Vomiero and Zafar Hussain Ibupoto

Email: alberto.vomiero@unive.it, zaffar.ibhupoto@usindh.edu.pk

Calculation (S2): Calculation of supercapacitor of 1D $NiCo_2O_4$ nanorods and its 0D nanoparticles

The calculations of Specific Capacitance C_s and energy density was done according to the published work [1] using the following mathematical relations:

$$C_s = \frac{I \times \Delta t}{m \times \Delta V}$$

Specific capacitance is C_s, I as current, Δt discharge time, ΔV potential range, m mass of deposited material onto GCE

Whereas energy density was calculated as:

$$E_d = \frac{C_s \times (\Delta V^2)}{2}$$

E_d as energy density, speiifc caapciatnec as Cs, ΔV^2 change in potential

Power density was measured as follows [1]:

$$P_d = \frac{E}{\Delta t}$$

P_d represents the power density; E is the energy and Δt discharge time.

Asymmetric supercapacitor was fabricated using two electrodes set up involving positive electrode $NiCo_2O_4$ nanostructures prepared with 2 mL of lemon juice and negative electrode of activated carbon (AC) in 3.0M KOH electrolytic solution. Commercial activated carbon was used for the development of negative electrode during two electrode configuration for the asymmetric device system. The slurry of activated carbon was prepared by dispersing 17 mg of Ac into 3:1 volume of ethanol and the deionized water. In this mixture 100µL of 5% Nafion was also added. The well dispersed slurry was achieved by sonication for 10 min. The anode of $NiCo_2O_4$ and cathode of AC was developed onto GCE respectively. The asymmetric supercapacitor was described by following configuration of $NiCo_2O_4$ sample 2//AC ASC. The balancing of voltammetric charges for the prepared $NiCo_2O_4$ sample 2 and AC was done with calculation of masses of two electrode by following relationship as previously reported Q+ = Q– equation [2].

$m+ m- = C_s- \Delta V- C_s+\Delta V+$.

Here: m±, Cs±, and ΔV± describes the mass, specific capacitance C_s, and potential range of $NiCo_2O_4$ sample 2 (+) and AC (−) electrodes, respectively. The estimated total mass of m+/m−

was about 0.17 mg in $NiCo_2O_4$ sample 2//AC ASC. For the calculation of C_s, and energy density and power density the total mass was calculated as per the reported work [3].

$$C_s = \frac{4 \times I \times \Delta t}{m \times \Delta V}$$

C_s represents specific capacitance, I current, discharge time Δt, potential change ΔV, loaded mass as m.

Energy density was calculated as:

$$E_d = \frac{C_s \times (\Delta V^2)}{7.2}$$

E_d is energy, C_s as specific capacitance, potential variation ΔV^2

The power density was determined by [2]:

$$P_d = \frac{C_s \times 3600}{\Delta t}$$

Here P_d is the power density, C_s is the specific capacitance and the discharge time is Δt

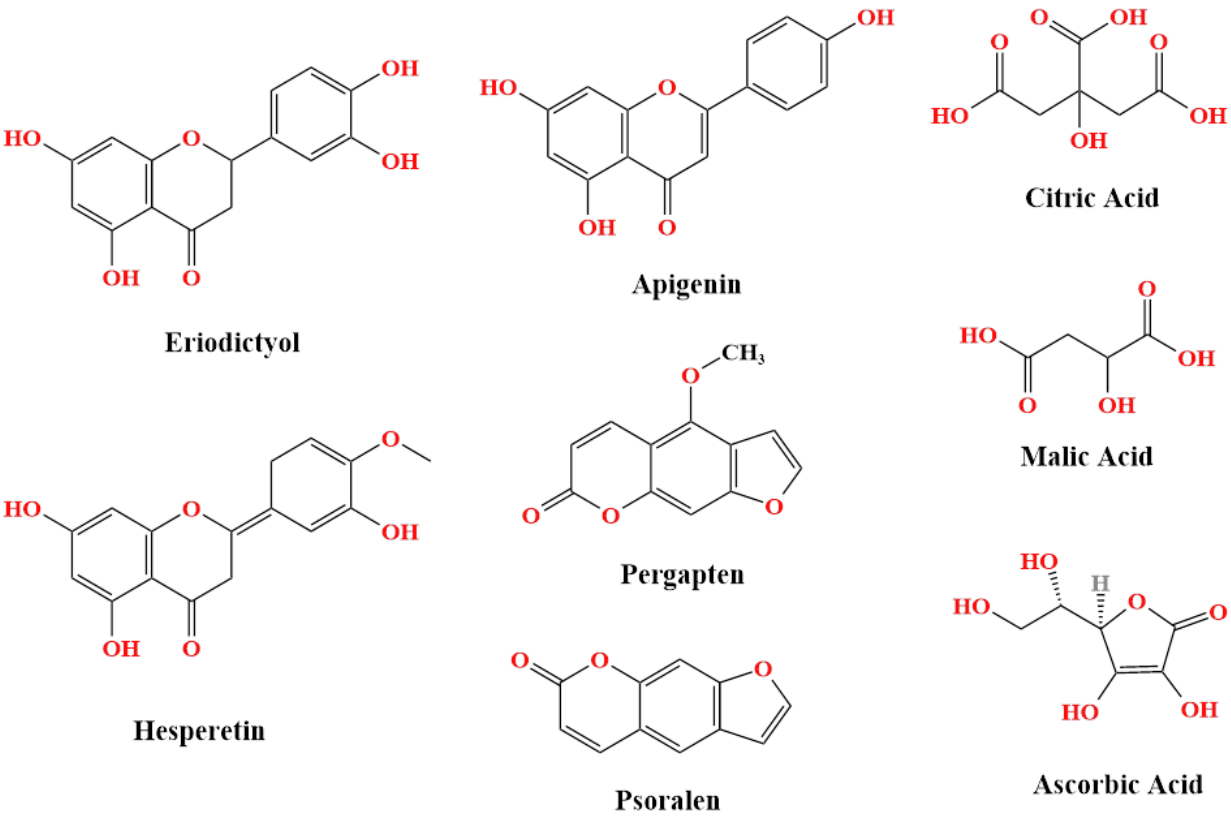

Scheme (S1): Chemical compounds in the lemon juice.

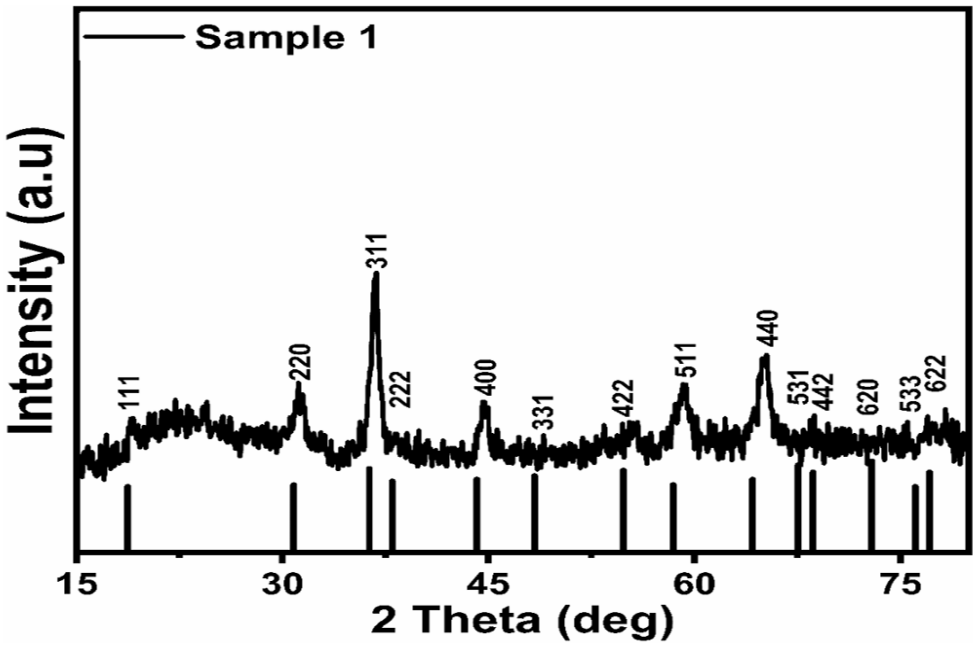

Figure S1: XRD diffraction patterns of sample 1 prepared with 0.5 mL of citrus lemon juice

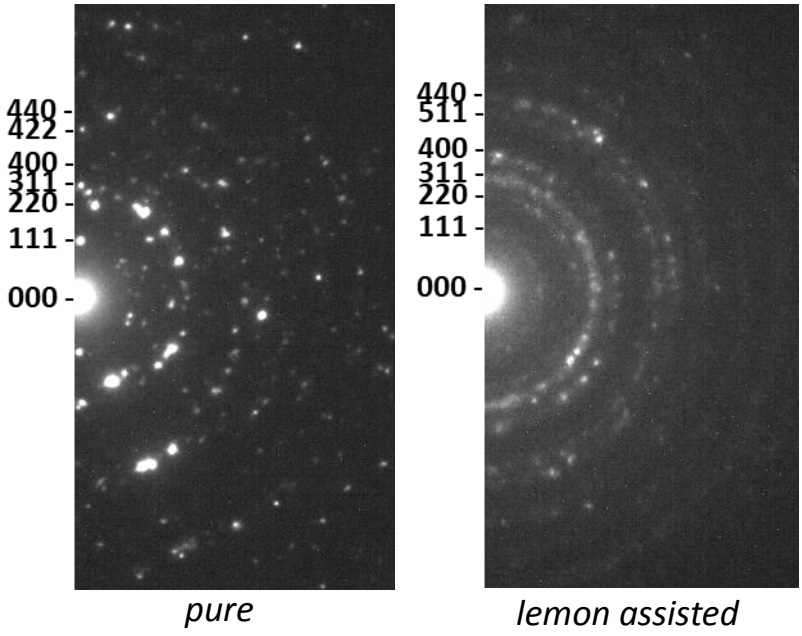

Figure S2: SAED patterns of pure $NiCo_2O_4$ and lemon assisted $NiCo_2O_4$ nanostructures

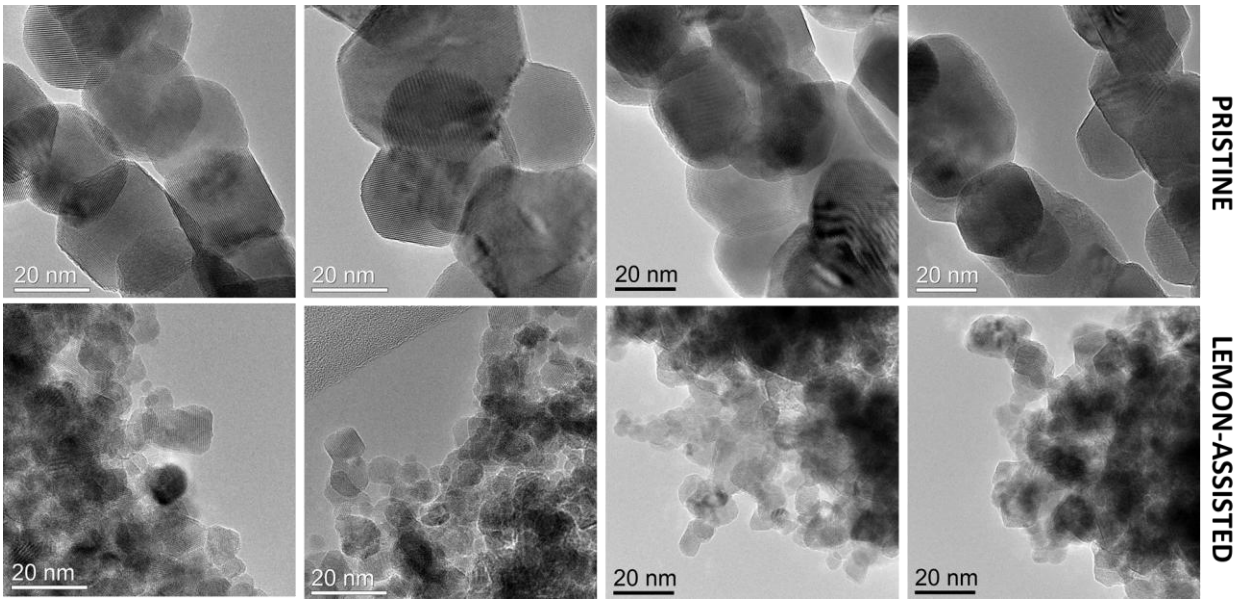

Figure S3: TEM micrographs of pure (top) and lemon-assisted (bottom) $NiCo_2O_4$

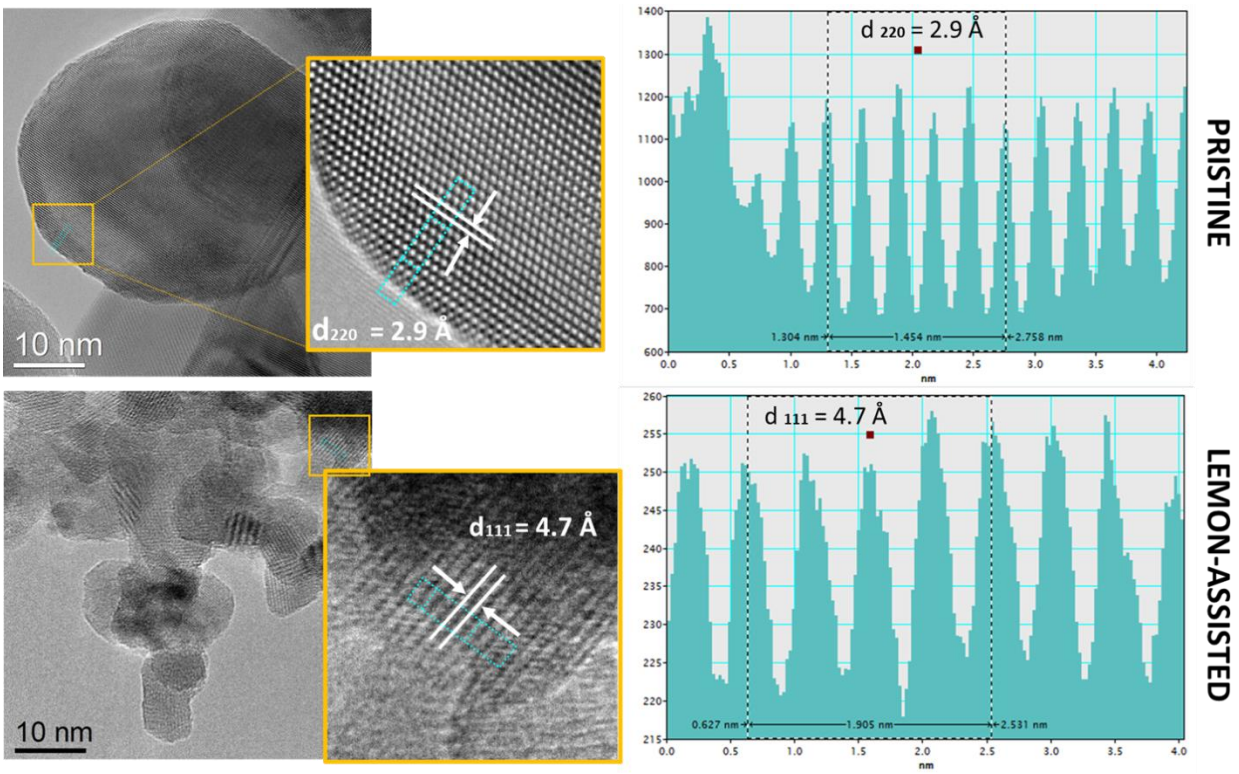

Figure S4: HRTEM micrographs of pure (top) and lemon-assisted (bottom) $NiCo_2O_4$ with corresponding intensity profiles taken in blue squared area of HRTEM images

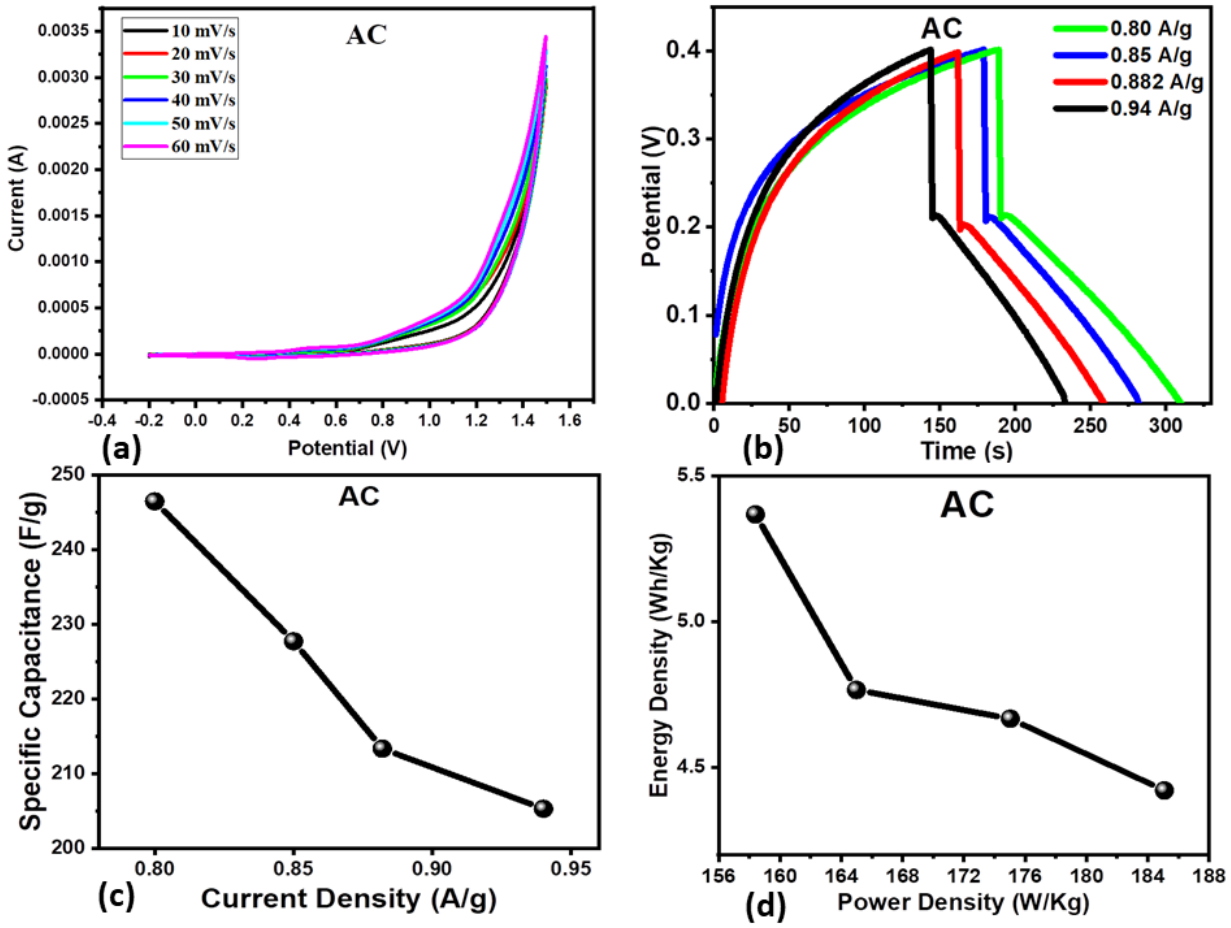

Figure S5: Various CV curves of activated carbon (AC) at various scan rates in 3.0M KOH, (b) GCD curves at different current density for AC, (c) specific capacitance of AC, (d) energy density and power density calculated values of AC

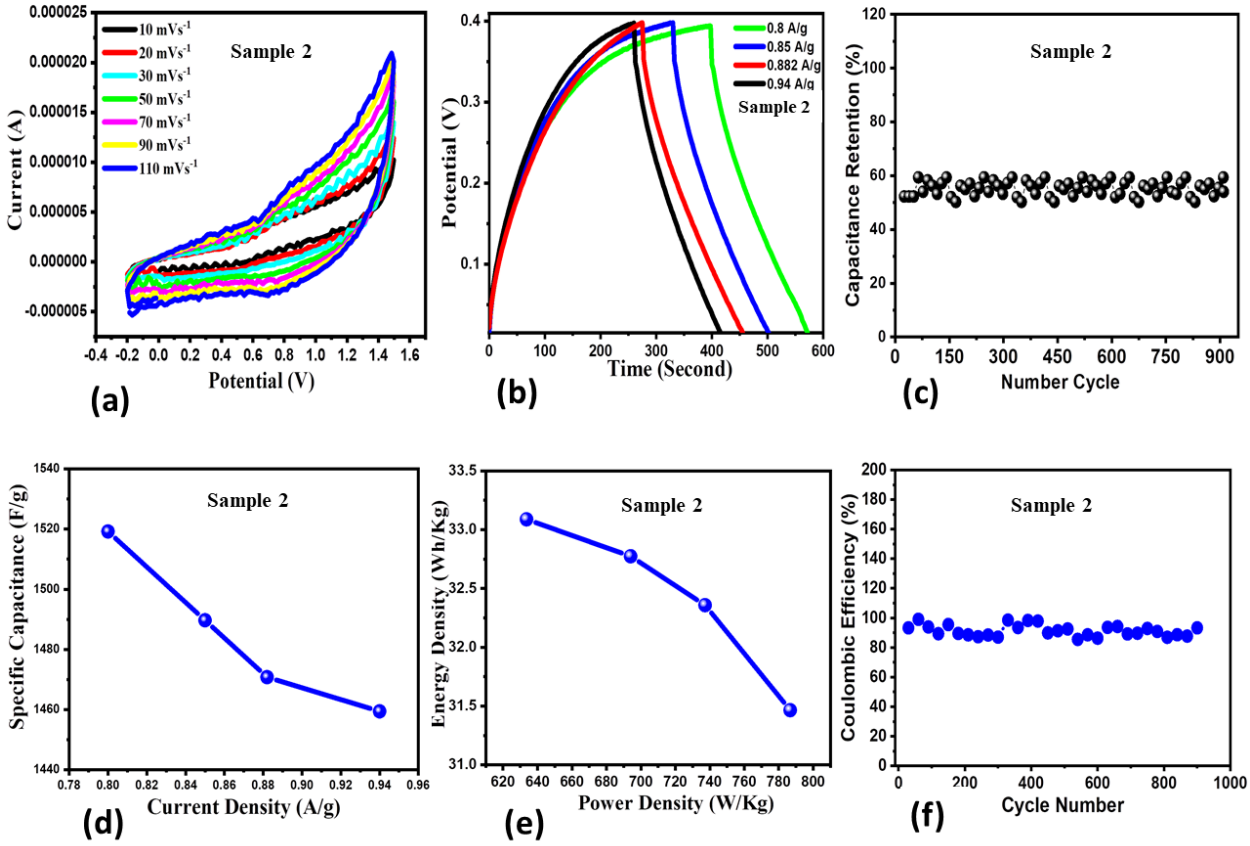

Figure S6: Various CV curves of $NiCo_2O_4$ (sample 2) at different scan rates in 3.0M KOH, (b) GCD curves at different current density for $NiCo_2O_4$ (sample 2), (c) Cycling stability of $NiCo_2O_4$ (sample 2), (d) specific capacitance of $NiCo_2O_4$ (sample 2) from GCD curves, (e) Energy density of $NiCo_2O_4$ (sample 2), (f) Columbic efficiency of $NiCo_2O_4$ (sample 2) during cycling stability.

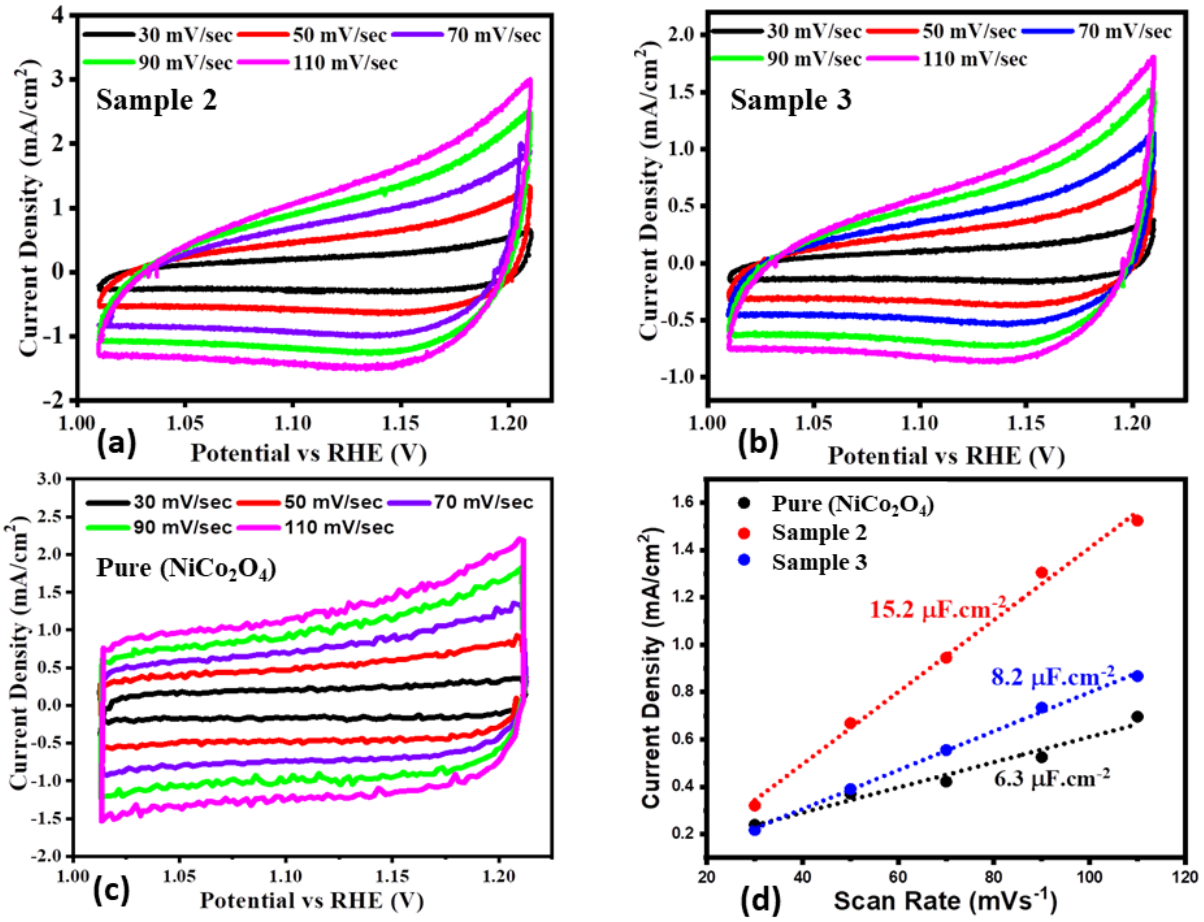

Figure S7: Different CV curves at variosu scan rates in 1.0M KOH for (a) pristine $NiCo_2O_4$ nanostructure, (b) $NiCo_2O_4$ (sample 2), (c) $NiCo_2O_4$ (sample 3), (d) caluclated ECSA from non-Faradic region of estimated CV curevs for pristine $NiCo_2O_4$ nanostructure, $NiCo_2O_4$ (sample 2), $NiCo_2O_4$ (sample 3).

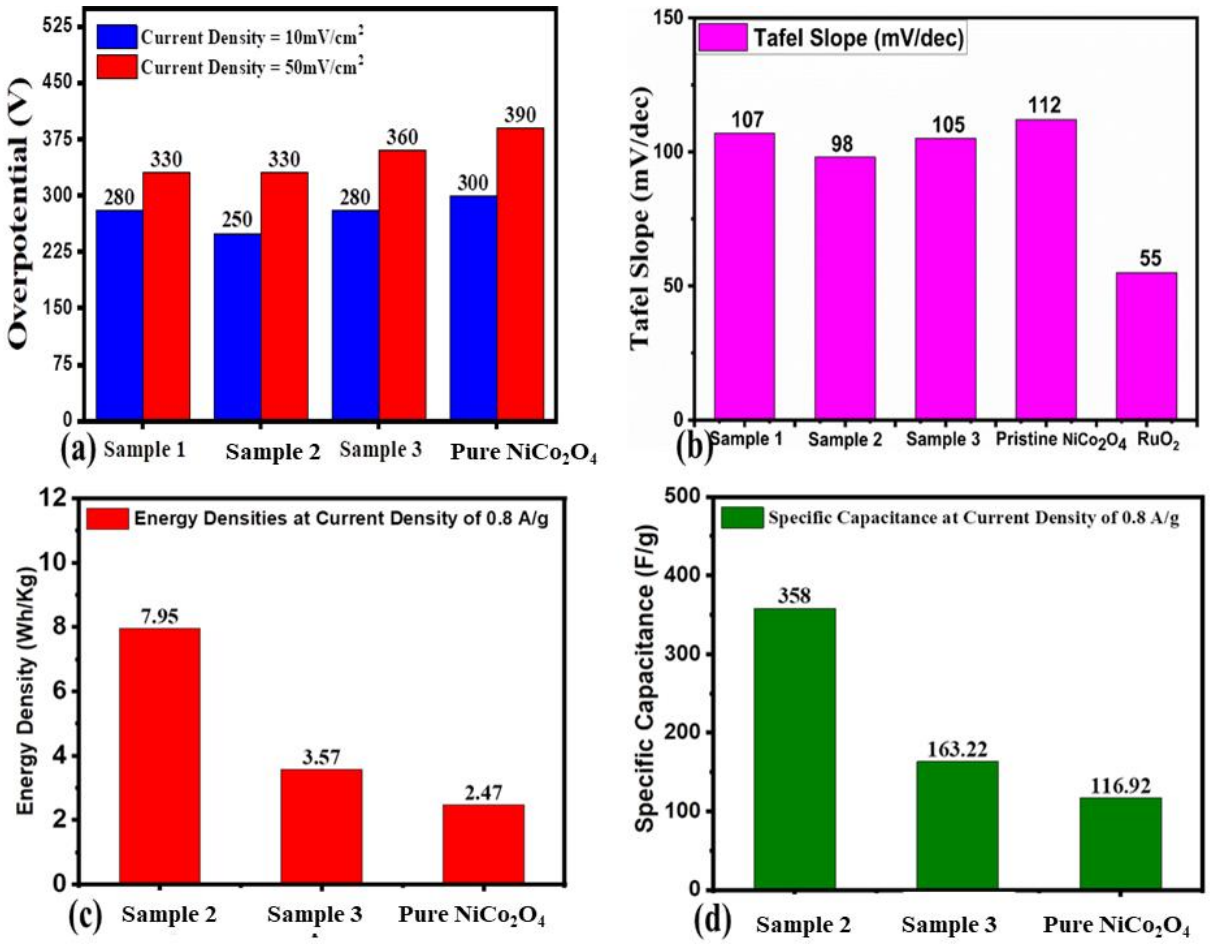

Figure S8: Bar graph view (a) overpotential at 10 and 50 $mAcm^{-2}$ for RuO_2, pure $NiCo_2O_4$ nanostructure, $NiCo_2O_4$ (sample 2), $NiCo_2O_4$ (sample 3), (b) Tafel slope for RuO_2, pristine $NiCo_2O_4$ nanostructure, $NiCo_2O_4$ (sample 2), $NiCo_2O_4$ (sample 3), (c) Energy density of supercapacitor for pristine $NiCo_2O_4$ nanostructure, $NiCo_2O_4$ (sample 2), $NiCo_2O_4$ (sample 3), (d) specific capacitance (Cs) for pristine $NiCo_2O_4$ nanostructure, $NiCo_2O_4$ (sample 2) and (sample 2).

Table S1:

PURE

Ni 2p3/2								
Band	Pos	PosSep	B_FWHM	FWHM	Height	%Gauss	Area	%Area
1	854.03	0	1.8	1.8	2730	90	5480	28.34
2	855.75	1.73	1.86	1.86	2442	100	4830	24.98
3	857.02	3	2.08	2.08	644	90	1492	7.72
4	861.11	7.08	4.68	4.68	1379	80	7532	38.96

Co 2p3/2								
Band	Pos	PosSep	B_FWHM	FWHM	Height	%Gauss	Area	%Area
1	779.54	0	2.2	2.2	6105	80	15681	54.97
2	781.39	1.85	2.24	2.24	2627	80	6855	24.03
3	784.21	4.67	4.55	4.55	780	100	3781	13.25
4	788.93	9.39	4	4	495	90	2212	7.76

O 1s								
Band	Pos	PosSep	B_FWHM	FWHM	Height	%Gauss	Area	%Area
1	529.43	0	1.11	1.11	9630	80	12480	61.02
2	531.13	1.7	1.54	1.54	3977	100	6509	31.82
3	532.69	3.26	1.6	1.6	820	90	1464	7.16

1L

Ni 2p3/2								
Band	Pos	PosSep	B_FWHM	FWHM	Height	%Gauss	Area	%Area
1	853.95	0	1.8	1.8	2230	100	4273	29.14
2	855.67	1.73	1.8	1.8	1889	100	3619	24.69
3	856.9	2.95	1.7	1.7	521	100	944	6.44
4	860.85	6.9	5.5	5.5	978	96	5825	39.73

Co 2p3/2								
Band	Pos	PosSep	B_FWHM	FWHM	Height	%Gauss	Area	%Area
1	779.29	0	2.02	2.02	3274	100	7045	53.88
2	781.09	1.8	2.3	2.3	1722	80	4617	35.31
3	784.07	4.79	4.5	4.5	192	100	918	7.02
4	788.81	9.52	4.58	4.58	101	100	494	3.78

O 1s								
Band	Pos	PosSep	B_FWHM	FWHM	Height	%Gauss	Area	%Area
1	529.25	0	1.2	1.2	6083	90	8139	47.59
2	531.08	1.83	1.82	1.82	3078	90	6234	36.45
3	532.53	3.27	1.5	1.5	1562	80	2731	15.96

Table S2: Calculated average crystallite size of pure $NiCo_2O_4$ and sample 1, sample 2 and sample 3.

Sample ID	**Height**	**FWHM**	**Crystalline size (nm)**
Pure $NiCo_2O_4$	44.61	0.26	14
Sample 1	36.84	0.28	16
Sample 2	45.03	0.25	14
Sample 3	44.06	0.12	18

Table S3: The calculated various supercapacitor indicators pure $NiCo_2O_4$ nanostructure (sample 2), $NiCo_2O_4$ (sample 3)

Samples	**Current Density (Ag^{-1})**	**Specific Capacitance (Fg^{-1})**	**Energy Density (Wh kg^{-1})**	**Power Density (W kg^{-1})**	**Columbic Efficiency (%)**	**Capacitance Retention (%)**
Sample 2	0.8	358	8	160	70%	100-94%
	0.85	284	6	167		
	0.882	126	3	176		
	0.94	118	3	188		
Sample 3	0.8	163	4	159	64%	108-83%
	0.85	154	3	169		
	0.882	149	3	175		
	0.94	60	1	183		
Pure ($NiCo_2O_4$)	0.8	117	2	156	43%	90-61%
	0.85	113	2	166		
	0.882	112	2	171		
	0.94	109	2	183		

Table S4: Supercapacitor performance evaluation of as synthesized $NiCo_2O_4$ nanostructure with lemon juice (sample 2) with reported supercapacitor based on $NiCo_2O_4$

Material	**Specific Capacitance (Fg^{-1})**	**Current Density (Fg^{-1})**	**Potential Window**	**Energy Density ($Wh\ kg^{-1}$)**	**Power Density ($W\ kg^{-1}$)**	**Reference**
NCO@MWCNT	374 F/g	2 A/g	-0.5 to 2.2V	95	3964	4
MWCNTs	84 F/g	0.6 A/g	-0.5 to 2.2V	21	6237	4
NCO//MWCNT	157 F/g	0.6 A/g	-0.5 to 2.2V	40	2816	4
NCO@MWCNT//MWCNT	242 F/g	0.6 A/g	-0.5 to 2.2V	61	2837	4
NiCoF	50.0	1 A/g	0 to 1 V	-	-	5
NiCuF	44	1 A/g	0 to 1 V	-	-	5
NC6	1294.25	10 A/g	0.4	-	-	6
NC10	687.20	10 A/g	0.4	-	-	6
Ni–Co–O–1	568	20 A g	0 to 0.5 V	19.72	5000	7
Ni–Co–O–2	532	20 Ag	-	-	-	7
$NiCo_2O_4$ (Lemon juice)	**358**	**0.8 A/g**	**0 to 0.4 V**	**7.96**	**160**	**This Work**

Table S5: Measured indicators for asymmetric supercapacitor using two electrode configuration of $NiCo_2O_4$ (sample 2) for practical applications

Samples	Current Density (Ag^{-1})	Specific capacitance (Fg^{-1})	Energy density ($Wh\ kg^{-1}$)	Power Density ($W\ kg^{-1}$)	Columbic Efficiency (%)	Capacitance Retention (%)
Sample 2	0.8	1519	33	634	100-84%	64-52% (900 Cycles)
	0.85	1490	33	694		
	0.882	1471	32	737		
	0.94	1459	31	787		

Table S6: Fitting values of EIS for charge transfer and double layer capacitance for pristine $NiCo_2O_4$ nanostructure, $NiCo_2O_4$ (sample 2), $NiCo_2O_4$ (sample 3)

Samples	Charge Transform Resistance (Rct in Ω)	Double Layer Capacitor (Cdl in Farad)
Pristine $NiCo_2O_4$	968	0.32
Sample 2	165	2.28
Sample 3	547	0.74

Table S7: The summary of OER activity performance of lemon juice assisted $NiCo_2O_4$ nanostructures with recently reported electrocatalysts in 1.0 M KOH.

Catalyst	**Over potential (mV) @ 10 mA/cm^2**	**Electrolyte**	**References**
$NiCo_2O_4$@Graphene Nano sheets	383	1.0 M KOH	8
NiOx/$NiCo_2O_4$/Co_3O_4	315	1.0 M KOH	9
$NiCo_2O_4$/CoO/graphite	323	1.0 M KOH	10
MOF derived-$NiCo_2O_4$/NiO	430	1.0 M KOH	11
P-doped $NiCo_2O_4$ on Ni-Foam	300	1.0 M KOH	12
Co_8FeS_8/CoS@CNT	278	1.0 M KOH	13
CoSx/MoS_2	347	1.0 M KOH	14
$NiCo_2O_4$/NiO	360	1.0 M KOH	15
$Co_xNi_{1-x}S_2$ (CNS)/RGO	290	1.0 M KOH	16
3D core–shell $NiCo_2O_4$@CoS/NF	290	1.0 M KOH	17
CoFe/Co_8FeS_8/CNT	290	1.0 M KOH	18
$NiCo_2O_4$/NiO hexagonal rods	285	1.0 M KOH	19
Ni_3S_2/MoS_2 (NiMoS)	260	1.0 M KOH	20
Ni_3N-NiMoN	277	1.0 M KOH	21
Co_3O_4@CMC	290	1.0 M KOH	22
Lemon juice assisted $NiCo_2O_4$ material	**250**	**1.0 M KOH**	**Present Work**

References

[1] E. Jokar & A. zad & S. Shahrokhian, J Solid State Electrochem 2015, 19, 269–274.

[2] Y. Liu, Y. Zheng, Q. Xu, Y. Shi, Z. Tian, R. wang, G. Zhang, J. Chen, Z. Wang, W. Zheng, Chem. Eng. J. 2020, 387, 12412-21.

[3] C.Young, R. R. Salunkhe, S. M. Alshehri,T. Ahamad, Z. Huang, J. Henzie, and Y. Yamauchi, J. Mater. Chem. A, 2017, 5, 11834-11839.

[4] M. Pathak, J. R. Jose, B. Chakraborty, and C. S. Rout, The Journal of Chemical Physics, 2020, 152, 064706.

[5] B. Bhujun, M. T. Tan, and A. S. Shanmugam, Results in Physics, 2017, 7, 345-353.

[6] M. Kaur, P. Chand, and H. Anand, Journal of Energy Storage, 2022, 52, 104941.

[7] H. Wang, Q. Gao, and L. Jiang, small, 2011, 7, 2454-2459.

[8] Z. Li, B. Li, J. Chen, Q. Pang, P. Shen. Int. J. Hydrogen Energy., 2019, 44, 16120–16131.

[9] J. Chen, Y. Ling, Z. Lu, X. Huai, F. Qin, Z. Zhang. Electrochim. Acta. 2019, 322, 134753.

[10] N. Srinivasa, L. Shreenivasa, P.S. Adarakatti, J.P. Hughes, S.J. Rowley-Neale, C.E. Banks, S. Ashoka, RSC Adv. 2019, 9, 24995–25002.

[11] Y. Wang, Z. Zhang, X. Liu, F. Ding, P. Zou, X. Wang, Q. Zhao, H. Rao. ACS Sustainable Chem. Eng. 2018, 6, 12511–12521.

[12] W. Chu, Z. Shi, Y. Hou, D. Ma, X. Bai, Y. Gao, N. Yang. ACS Appl. Mater. Interfaces, 2020, 12, 2763–2772.

[13] B. Wang, Y. Chen, X. Wang, X. Zhang, Y. Hu, B. Yu, D. Yang, W. Zhang. J. Power Sources. 2020, 449, 227561.

[14] L. Yang, L. Zhang, G. Xu, X. Ma, W. Wang, H. Song, D. Jia. ACS Sustainable Chem. Eng. 2018, 6, 12961–12968.

[15] C. Mahala, M. Basu. ACS Omega 2017, 2, 7559–7567.

[16] Y.-R. Hong, S. Mhin, K.-M. Kim, W.-S. Han, H. Choi, G. Ali, K.Y. Chung, H.J. Lee, S.-I. Moon, S. Dutta, S. Sun, Y.-G. Jung, T. Song, H. Han. J. Mater. Chem. A 2019, 7, 3592–3602.

[17] S. Adhikari, Y. Kwon, and D. H. Kim. Chemical Engineering Journal, 2020, 402, 126192.

[18] B. Wang, Y. Hu, B. Yu, X. Zhang, D. Yang, Y. Chen. J. Power Sources., 2019, 433, 126688.

[19] Y. Yuan, L. Sun, Y. Li, W. Zhan, X. Wang, X. Han, Inorg. Chem. 2020, 59, 4080–4089.

[20] C. Wang, X. Shao, J. Pan, J. Hu, X. Xu. Appl. Catal. B., 2020, 268, 118435.

[21] A. Wu, Y. Xie, H. Ma, C. Tian, Y. Gu, H. Yan, X. Zhang, G. Yang, and H. Fu. Nano Energy, 2018, 44, 353-363.

[22] A. L. Bhatti, A. Tahira, A. Gradone, R. Mazzaro, V. Morandi, M.I. Abro, A. Nafady, K. Qi. Electrochimica Acta, 2021, 398, 139338.